

Chapter 15

Unilateral and Bilateral Rehabilitation of the Upper Limb Following Stroke via an Exoskeleton

Jacob Rosen, Dejan Milutinović, Levi M. Miller, Matt Simkins, Hyunchul Kim, and Zhi Li

Abstract Recent studies reported positive effects of bilateral arm training on stroke rehabilitations. The development of novel robotic-based therapeutic interventions aims at recovery of the motor control system of the upper limb, in addition to the increase of the understanding of neurological mechanisms underlying the recovery of function post stroke. A dual-arm upper limb exoskeleton EXO-UL7 that is kinematically compatible with the human arm is developed to assist unilateral and bilateral training after stroke. Control algorithms are designed and implemented to improve the synergy of the human arm and the upper limb exoskeleton. Clinical studies on the robot-assisted bilateral rehabilitations show that both the unilateral and bilateral training have a positive effect on the recovery of the paretic arm. Bilateral training outperforms unilateral training by a significant improvement of motion range and movement velocities.

Keywords Unilateral/bilateral stroke rehabilitation • Upper limb exoskeleton • Human arm • Kinematics • Dynamics

J. Rosen (✉) • D. Milutinović • M. Simkins • Z. Li
Department of Computer Engineering, University of California, Santa Cruz, CA 95064, USA
e-mail: rosen@ucsc.edu; dejan@soe.ucsc.edu; msimkins@soe.ucsc.edu; zli12@ucsc.edu

L.M. Miller
Carbon Design Group, Seattle, WA, USA
e-mail: levimakaio@gmail.com

H. Kim
Apple Inc., Cupertino, CA, USA
e-mail: hyunchul78@gmail.com

15.1 Introduction

Stroke is a leading cause of long-term neurological disability and the top reason for seeking rehabilitative services in the U.S. Challenges in rehabilitation after stroke, especially in the chronic phase are two-fold: the first is the development of systems for intense delivery of targeted rehabilitative interventions based on neural plasticity that will facilitate recovery and the second is to understand neural reorganization that facilitates the recovery of function. Whereas in the acute phase post stroke, medical management focuses on containing and minimizing the extent of the injury, in the chronic phase post stroke, neural plasticity induced by learning/training is the fundamental mechanism for recovery. The development of novel robotic based therapeutic interventions aims at facilitating neural plasticity and inducing sustainable recovery of the motor control system of the upper limb. In addition, studies on the synergy of the human arm and wearable robotic system (e.g., an upper limb exoskeleton) improve the understanding of neurological mechanisms which aim to maximize the recovery of function post stroke.

15.1.1 *Bilateral Robotic System and Treatment*

Research studies suggest that manual bilateral movements in which both arms and hands move simultaneously in a mirror image fashion or work simultaneously while performing a bilateral task have profound effects on the reorganization of the neural system due to inherent brain plasticity. Using such a therapeutic approach for stroke patients is based on the understanding that both brain hemispheres (damaged and undamaged) are going through a natural recovery process, as well as neural reorganization following a learning-based therapy. In spite of significant scientific evidence, translating a mirror image bilateral therapeutic approach into an intense (high dosage) physical rehabilitation treatment regime has been difficult. A therapist administering this regime is challenged to simultaneously control the 16 degrees of freedom (DOF) of both arms (14 DOF) and hands (2 DOF limited to 3-point chuck type grasping).

When considering bilateral symmetric movement training as an option for therapy, there are two aspects to its efficacy. The first aspect relates to neuroscience. Based on experiments relating to bilateral symmetric manual coordination using trans-cranial magnetic stimulation and kinematic modeling, symmetric movement might reduce inhibitions between the left and right hemispheres [1, 2]. In other words, bilateral symmetric movements have been found to increase cross-talk in the corpus callosum. In that vein, multiple studies have demonstrated the effectiveness of mirror therapy. Using mirror therapy, stroke survivors were able to improve function based on the optical illusions of their paretic arm moving normally [3, 4]. Based on such research, it has been proposed that symmetric movement training might exploit such coupling thereby allowing for an increased use of undamaged

ipsilateral projections [5]. In this way, symmetric movement training might improve the recovery process after a CVA. With respect to clinical outcomes, the results are somewhat mixed. It is admittedly difficult to detect improvement. For individuals who have chronic motor impairment, improvement after therapy is often subtle. Standard care, unilateral and bilateral movement training have all been shown to result in some improvement. However, distinguishing between training modalities is difficult and the differences are small. To that end, there is virtually no data (such as brain imaging) relating to neurological activity and bilateral therapy. For these reasons, it remains uncertain if bilateral symmetric therapy is truly better than unilateral therapy in the sense that there is more or less cross-talk between the hemispheres. More to the point, there is no conclusive evidence that bilateral symmetric movement training has a neurological basis.

Beyond neurological considerations, there are factors that distinguish the efficacy of bilateral and unilateral movement training. Bilateral movement training was shown to have better results than unilateral movement training in terms of the range of motion (ROM). One explanation for this difference is that the paretic arm was provided robotic assistance, while in the unilateral case, no assistance was provided. Subjects also reported that they preferred assistance [6]. While it is true that a robot can provide assistance for unilateral movement training, the control algorithms and game designs become much more constrained. During movement training, providing assistance that moves the arm through large angles might make the therapy feel unpredictable and might raise safety concerns. However, when the paretic arm is made to move symmetrically with the less affected arm, the subject is in control, and the game play is more predictable and the assistance is more natural. Therefore, bilateral training provides a flexible control paradigm for unstructured assistance.

There are two approaches for bilateral training. One involves full assistance [7] and the other requires partial assistance [6]. For full assistance, the paretic arm is forced into symmetric motion. Using this approach, the subjects may focus entirely on their less affected limb in order to play therapy games or to complete tasks. The subjects might use a minimum of effort to move their paretic arm, and what movements they do make will have little to no effect on the game play or task completion. Bilateral symmetric movement training with partial assistance allows the robot to provide some help for the paretic arm. However, the subjects cannot quite play the game or complete the task with their paretic arm unless they provide some voluntary effort. Subjects also perceived better outcomes for full assistance than partial assistance [6].

Bilateral symmetric movement training does have the potential to aggravate spasticity [6]. The cause for this relates to the speed of motion. It is known that rapid flexion and extension of spastic joints can intensify existing spasticity. This in turn can result in pain, weakness, and reduced coordination. When subjects perform symmetric movements, their less affected arm might move too rapidly. In turn, as the robot attempts to maintain symmetry, the paretic arm might move too quickly thus aggravating spasticity. The largest effects were evident in the hand. Therefore, bilateral symmetric movement is recommended for individuals who have

mild spasticity. If robotic training is used with assistance, be it bilateral or unilateral, care is needed not to move the paretic arm too fast.

15.1.2 Robot-Assisted Stroke Rehabilitation

Recently research results have demonstrated that robotic devices can deliver effective rehabilitation therapies to patients suffering from the chronic neuromuscular disorders [8–10]. MIT-MANUS is one of the successful rehabilitation robots which adopted back-drivable hardware and impedance control as a robot control system [11]. ARMin is a 7-DOF upper limb exoskeleton developed in ETH Zurich and the University of Zurich. This robot provides visual, acoustic and haptic interfaces together with cooperative control strategies to facilitate the patient's active participation in the game. The lengths of the upper arm, lower arm, hand and the height of the device are adjustable to accommodate patients of different sizes. The rehabilitation site and robotic system are wheelchair accessible. Pneu-WREX is a 6-DOF exoskeleton robot developed in UC Irvine. This robotic system adopted pneumatic actuators [12]. Although the pneumatic actuator is harder to control due to its non-linear characteristics, it produces relatively large forces with a low on-board weigh [13]. The robot interacts with the virtual-reality game T-WREX based on a Java Therapy 2.0 software system. Arizona State University researchers developed a robotic arm, RUPERT (Robotic Upper Extremity Repetitive Therapy) targeting cost-effective and light-weight stroke patient rehabilitation [14, 15]. The device provides the patient with assistive force to facilitate fluid and natural arm movements essential for the activities of daily living. The controller for the pneumatic muscles can be programmed for each user to improve their arm and hand flexibility, as well as strength by providing a repetitive exercise pattern. In our previous work [16], the seven-DOF exoskeleton robot UL-EXO7 [8, 17, 18] was exploited as a core mechanical system for the long-term clinical trial of the bilateral and unilateral rehabilitation program. The controllers equipped in UL-EXO7 provided the assistive force to help patients make the natural arm posture based on the work in [19, 20]. For the objective and fine-scale rehabilitation assessment, a new assessment metric, an efficiency index, was introduced to tell the therapist how close the patient's arm movements are to the normal subject's arm movements.

15.1.3 Objective and Paper Structure

This chapter describes the EXO-UL7 – an upper limb exoskeleton system and its clinical applications to bilateral stroke rehabilitation. Section 15.2 reviews the kinematic design of the EXO-UL7 with considerations in its compatibility with the kinematics of the human arm. Based on the kinematic modeling of the human

arm, the forward and inverse kinematics are derived. The control architectures are addressed, including the control algorithms for admittance control, gravity compensation, inter-arm teleoperation and redundancy resolution. Clinical studies on robot-assisted bilateral rehabilitations are presented in Sect. 15.3, with a comparison of the outcomes of unilateral and bilateral training.

15.2 An Upper Limb Exoskeleton: EXO-UL7

15.2.1 System Overview

The kinematics and dynamics of the human arm during activities of daily living (ADL) have been studied to determine specifications for exoskeleton design (see Fig. 15.1). Articulation of the exoskeleton is achieved by seven single-axis revolute joints which support 99% of the range of motion required to perform daily activities. Three revolute joints are responsible for shoulder abduction-adduction, flexion-extension and internal-external rotation. A single rotational joint is employed at the elbow, creating elbow flexion-extension. Finally, the lower arm and hand are connected by a three-axis spherical joint resulting in wrist pronation-supination, flexion-extension, and radial-ulnar deviation. As a



Fig. 15.1 The upper limb exoskeleton EXO-UL7 with seven DOFs, supporting 99% of the range of motion required to perform daily activities

human-machine interface (HMI), four six-axis force/torque sensors (ATI Industrial Automation, model-Mini40) are attached to the upper arm, the lower arm, the hand and the tip of the exoskeleton. The force/torque sensor at the tip of the exoskeleton allows measurements of the interactions between the exoskeleton and the environment [8, 9, 21].

15.2.2 Kinematic Design of the Upper Limb Exoskeleton EXO-UL7

15.2.2.1 Kinematic Modeling of the Human Arm

The upper limb exoskeleton EXO-UL7 is designed to be compatible with the human arm kinematics. The human arm is composed of segments linked by articulations with multiple degrees of freedom. It is a complex structure that is made up of both rigid bone and soft tissue. Although much of the complexity of the soft tissue is difficult to model, the overall arm movement can be represented by a much rigid body model composed of rigid links connected by joints. Three rigid segments, consisting of the upper arm, lower arm and hand, connected by frictionless joints, make up the simplified model of the human arm. The upper arm and torso are rigidly attached by a ball and socket joint. This joint enables shoulder abduction-adduction (abd-add), shoulder flexion-extension (flx-ext) and shoulder internal-external (int-ext) rotation. The upper and lower arm segments are attached by a single rotational joint at the elbow, creating elbow flx-ext. Finally, the lower arm and hand are connected by a 3-axis spherical joint resulting in pronation-supination (pron-sup), wrist flx-ext, and wrist radial-ulnar (rad-uln) deviation. Models of the human arm with seven DOFs have been widely used in various applications, including rendering human arm movements by computer graphics [22, 23], controlling redundant robots [24, 25], kinematic design of the upper limb exoskeletons [18, 26, 27], and biomechanics [28–30]. These models provide a synthesis of proper representation of the human and the exoskeleton arm as redundant mechanisms along with an adequate level of complexity.

The kinematics and dynamics of the human arm during activities of daily living (ADL) were studied in part to determine engineering specifications for the exoskeleton design [8]. Using these specifications, two exoskeletons were developed, each with seven DOFs. Each exoskeleton arm is actuated by seven DC brushed motors (Maxon) that transmit the appropriate torque to each joint utilizing a cable-based transmission. The mechanisms are attached to a frame mounted on the wall, which allows both height and distance between the arms to be adjusted. Articulation of the exoskeleton is achieved about seven single axis revolute joints – one for each shoulder abd-add, shoulder flx-ext, shoulder int-ext rotation, elbow flx-ext, forearm pron-sup, wrist flx-ext, and wrist rad-uln deviation. The exoskeleton joints are labeled 1–7 from proximal to distal in the order shown in Fig. 15.2. With seven joint rotations, there is one redundant degree of freedom.

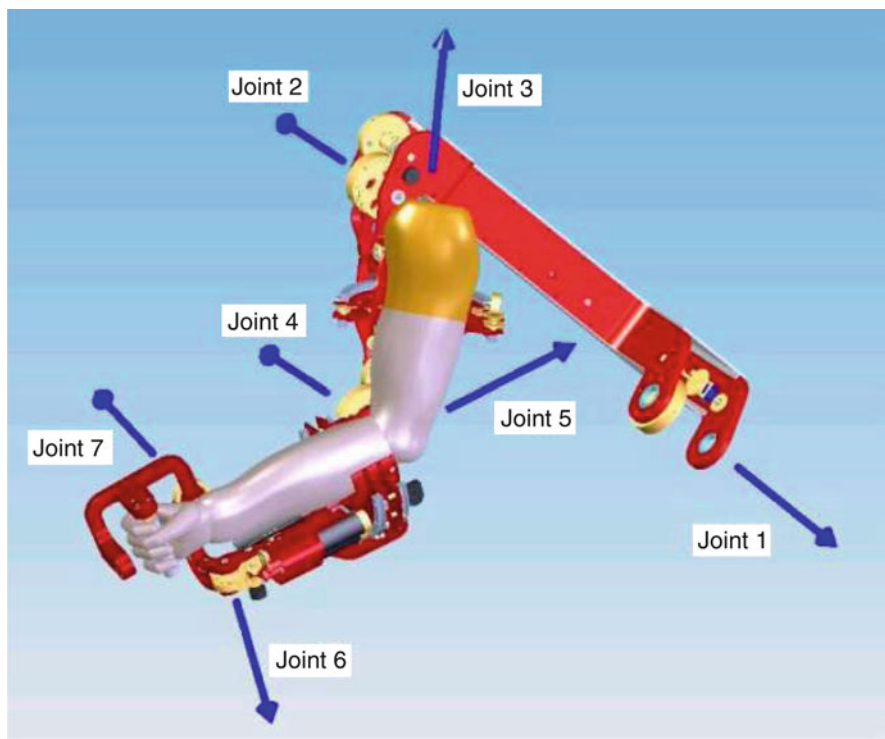


Fig. 15.2 Exoskeleton axes assignment relative to the human arm. Positive rotations about each joint produce the following motions: (1) combined flx/adb, (2) combined flx/add, (3) int rotation, (4) elbow flx, (5) forearm pron, (6) wrist ext, and (7) wrist rad dev

The fundamental principle in designing the exoskeleton joints is to align the rotational axis of the exoskeleton with the anatomical rotations axes. If more than one axis is at a particular anatomical joint (e.g. shoulder and wrist), the exoskeleton joints emulate the anatomical joint interaction at the center of the anatomical joint. Consistent with other work, the glenohumeral (G-H) joint is modeled as a spherical joint composed of three intersection axes [31]. The elbow is modeled by a single axis orthogonal to the third shoulder axis, with a joint stop to prevent hyperextension. Exoskeleton pron-sup takes place between the elbow and the wrist as it does. Finally, two intersecting orthogonal axes represent the wrist. The ranges of motion of the exoskeleton joints support 99 % of the ranges of motion required to perform daily activities [8].

Representing the ball and socket joint of the shoulder as three intersecting joints introduces singularities that are not present in the human arm model. A significant consideration in the exoskeleton design is the placement of singularities [24]. The singularity is a device configuration in which a DOF is lost or compromised as a result of the alignment of two rotational axes. In the development of a three DOF

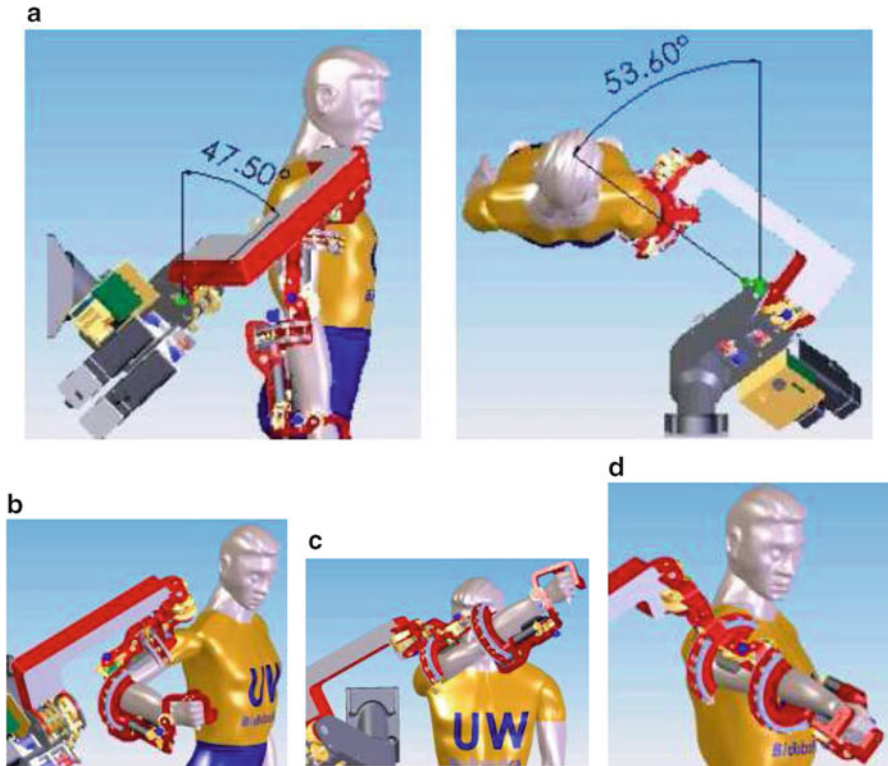


Fig. 15.3 Two singularities exist in the exoskeleton device, one when joints 1 and 3 align and the other when joints 3 and 5 align. (a) The orientation of joint 1 places the singularity at the shoulder in an anthropomorphically difficult place to reach. (b) Joints 1 and 3 align with simultaneous extension and abduction of the upper arm by 47.5° and 53.6° . (c) Similarly, the same singularity can be reached through flexion and adduction by 132.5° and 53.6° . (d) Alignment of joints 3 and 5 naturally occurs only in full elbow extension

spherical joint, the existence or nonexistence of singularities will depend entirely on the desired reachable workspace. Spherical workspace equal to or larger than a hemisphere will always contain singular positions. The challenge is to place the singularity in an unreachable, or near-unreachable location, such as the edge of the workspace. For the exoskeleton arm, singularities occur when joints 1 and 3 or joints 3 and 5 align. To minimize the frequency of this occurrence, the axis of joint 1 is positioned such that singularities with joint 3 take place only at locations that are anthropometrically hard to reach. For the placement shown in Fig. 15.3a, the singularity can be reached through simultaneous extension and abduction of the upper arm by 47.5° and 53.6° , respectively (see Fig. 15.3b). Similarly, the same singularity can be reached through flexion and adduction by 132.5° and 53.6° , respectively (see Fig. 15.3c). The singularity between joints 3

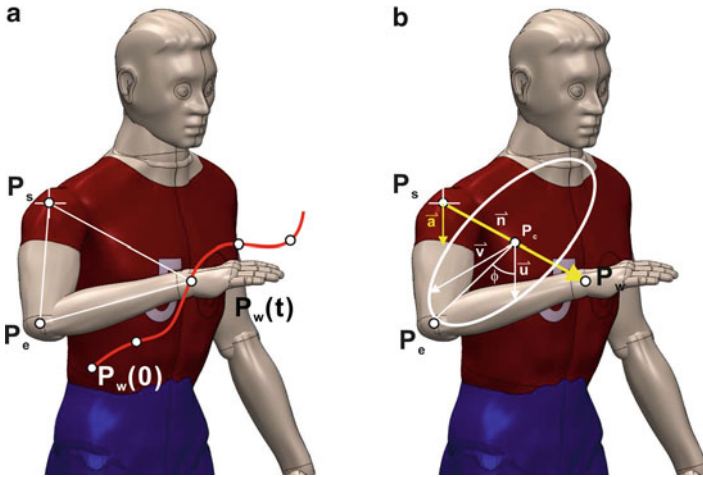


Fig. 15.4 (a) Given a fixed wrist position in a 3D workspace, the arm plane formed by the positions of the shoulder (P_s), the elbow (P_e) and the wrist (P_w) can move around an axis that connects the shoulder and the wrist due to the kinematic redundancy. (b) The redundant DOF can be represented by a swivel angle ϕ

and 5 naturally occurs only in full elbow extension, i.e., on the edge of the forearm workspace (see Fig. 15.3d). With each of these singularity vectors at or near the edge of the human workspace, the middle and majority of the workspace is free of singularities [8, 9].

15.2.2.2 Representation of the Redundant Degree of Freedom

Given the position (x, y, z) and the orientation $(\phi_x, \phi_y, \text{ and } \phi_z)$ of a target in a 3-dimensional (3D) workspace, the human arm has a redundant DOF which allows the elbow to move around an axis that goes through the center of the shoulder and the wrist joints. This redundant DOF provides the flexibility in human arm postures when completing the tasks defined in the 3D workspace. When applied to controlling the upper limb exoskeleton, a swivel angle is used to represent the redundant DOF. It specifies how much the elbow position pivots about the axis that goes through the center of shoulder and center of wrist, when the hand has a specific position and orientation.

As shown in Fig. 15.4, the arm plane is formed by the positions of the shoulder, the elbow and the wrist (denoted by P_s , P_e and P_w , respectively). The direction of the axis that the arm plane pivots about (denoted by \mathbf{n}) is defined as:

$$\mathbf{n} = \frac{P_w - P_s}{\|P_w - P_s\|} \tag{15.1}$$

Table 15.1 Denavit-Hartenberg (DH) Parameters for upper limb exoskeleton

Robot	$i - 1$	i	α_i	a_i	d_i	θ_i
Left arm	0	1	$\pi/2$	0	0	$\theta_1 + \pi - 32.94^\circ$
	1	2	$\pi/2$	0	0	$\theta_2 + \pi/2 - 28.54^\circ$
	2	3	$\pi/2$	0	0	$\theta_3 + \pi - 53.6^\circ$
	3	4	$\pi/2$	0	L_1	θ_4
	4	5	$-\pi/2$	0	0	$\theta_5 - \pi/2$
	5	6	$-\pi/2$	0	L_2	$\theta_6 + \pi/2$
	6	7	$\pi/2$	0	0	$\theta_7 + \pi$
Right arm	0	1	$\pi/2$	0	0	$\theta_1 - 32.94^\circ$
	1	2	$\pi/2$	0	0	$\theta_2 - \pi/2 - 28.54^\circ$
	2	3	$-\pi/2$	0	0	$\theta_3 - \pi - 53.6^\circ$
	3	4	$-\pi/2$	0	$-L_1$	θ_4
	4	5	$\pi/2$	0	0	$\theta_5 + \pi/2$
	5	6	$-\pi/2$	0	$-L_2$	$\theta_6 + \pi/2$
	6	7	$\pi/2$	0	0	$\theta_7 + \pi$

The plane orthogonal to \mathbf{n} can be determined given the position of P_e . P_c is the intersection point of the orthogonal plane with the vector $P_w - P_s$. $\mathbf{P}_e - \mathbf{P}_c$ is the projection of the upper arm ($\mathbf{P}_e - \mathbf{P}_s$) on the orthogonal plane. \mathbf{u} is the projection of a normalized reference vector \mathbf{a} onto the orthogonal plane, which can be calculated as:

$$\mathbf{u} = \frac{\mathbf{a} - (\mathbf{a} \cdot \mathbf{n})\mathbf{n}}{\|\mathbf{a} - (\mathbf{a} \cdot \mathbf{n})\mathbf{n}\|} \quad (15.2)$$

The swivel angle ϕ , represents the arm posture, can be defined by the angle between the vector $\mathbf{P}_e - \mathbf{P}_c$ and \mathbf{u} . The reference vector \mathbf{a} is suggested to be $[0, 0, -1]^T$ such that the swivel angle $\phi = 0^\circ$ when the elbow is at its lowest possible point [32].

15.2.2.3 The Forward and Inverse Kinematics of the Upper Limb Exoskeleton

This section derives the forward and inverse kinematics of the EXO-UL7 exoskeleton. Table 15.1 shows the Denavit-Hartenberg (DH) parameters of the upper limb exoskeleton, which are derived using the standard method (see [33]). The joint angle variables are θ_i ($i = 1, \dots, 7$). L_1 and L_2 are the length of the upper and lower arms, respectively. The forward kinematics derives the transformation matrix 0_7T , which provides the position and the orientation of the wrist of the exoskeleton with respect to the base frame T_{base} :

Table 15.2 Base rotation of the upper limb exoskeleton

	θ_X (°)	θ_Y (°)	θ_Z (°)
Left arm	132.5	45	90
Right arm	132.5	-45	90

$$\begin{aligned}
{}^7_{base}T &= T_{base} \cdot {}^0_1T \cdot {}^1_2T \cdot {}^2_3T \cdot {}^3_4T \cdot {}^4_5T \cdot {}^5_6T \cdot {}^6_7T \\
&= \begin{bmatrix} r_{11} & r_{12} & r_{13} & P_{wx} \\ r_{21} & r_{22} & r_{23} & P_{wy} \\ r_{31} & r_{32} & r_{33} & P_{wz} \\ 0 & 0 & 0 & 1 \end{bmatrix} \quad (15.3)
\end{aligned}$$

In order to move the singularity out of the range of the daily movements of the human arm, the bases of the two robotic arms of the upper limb exoskeleton are rotated according to Table 15.2. Note that θ_X , θ_Y and θ_Z represent the rotation about the X, Y and Z-axis, respectively. The transformation matrix for the base rotation is described in Eq. (15.4).

$$T_{base} = Rotx(\theta_X)Rotz(\theta_Y)Rotz(\theta_Z) \quad (15.4)$$

With the specification of the transformation matrix 0_7T , the inverse kinematics of the exoskeleton can be derived for the left and the right arm, respectively. The redundant DOF of the human arm can be constrained by specifying the elbow position ($P_e = [Pe_x, Pe_y, Pe_z]^T$).

Based on the shoulder position P_s , elbow position P_e , and wrist position P_w , θ_4 can be derived as:

$$W = \|P_w - P_s\| \quad (15.5)$$

$$c_4 = \frac{L_1^2 + L_2^2 - W^2}{2L_1L_2} \quad (15.6)$$

$$s_4 = \sqrt{1 - c_4^2} \quad (15.7)$$

$$\theta_4 = \pi - \text{Atan2}(s_4, c_4) \quad (15.8)$$

The transformation matrix 3_4T and its inverse ${}^3_4T^{-1}$ can be found based on θ_4 .

The transformation matrix without the base rotation, denoted ${}^7_{base}T$, can be found by:

$${}^0_7T = T_0^{-1} \cdot {}^7_{base}T = \begin{bmatrix} r'_{11} & r'_{12} & r'_{13} & {}^0_7P_{wx} \\ r'_{21} & r'_{22} & r'_{23} & {}^0_7P_{wy} \\ r'_{31} & r'_{32} & r'_{33} & {}^0_7P_{wz} \\ 0 & 0 & 0 & 1 \end{bmatrix} \quad (15.9)$$

Thus, the wrist position with respect to the rotated base is ${}^0_7P_w = [{}^0_7P_{wx}, {}^0_7P_{wy}, {}^0_7P_{wz}]^T$.

Similarly, the elbow position with respect to the rotated base, denoted by ${}^0_7P_e = [{}^0_7P_{ex}, {}^0_7P_{ey}, {}^0_7P_{ez}]^T$, is:

$$\begin{bmatrix} {}^0_7P_{ex} \\ {}^0_7P_{ey} \\ {}^0_7P_{ez} \\ 1 \end{bmatrix} = T_0^{-1} \cdot \begin{bmatrix} {}^{base}_7P_{ex} \\ {}^{base}_7P_{ey} \\ {}^{base}_7P_{ez} \\ 1 \end{bmatrix} \quad (15.10)$$

Note that ${}^0_7P_e = {}^0_4P_e$ and

$${}^0_4T = {}^0_1T \cdot {}^1_2T \cdot {}^2_3T \cdot {}^3_4T = \begin{bmatrix} {}^0_4R & {}^0_4P_{ex} \\ & {}^0_4P_{ey} \\ & {}^0_4P_{ez} \\ 0 & 0 & 0 & 1 \end{bmatrix} = \begin{bmatrix} {}^0_4R & L_1c_1s_2 \\ & L_1c_2 \\ & L_1s_1s_2 \\ 0 & 0 & 0 & 1 \end{bmatrix} \quad (15.11)$$

For the both arms,

$$c_2 = \frac{{}^0_4P_{ey}}{L_1} \quad (15.12)$$

For the left arm,

$$s_2 = \sqrt{(1 - c_2^2)} \quad (15.13)$$

For the right arm,

$$s_2 = -\sqrt{(1 - c_2^2)} \quad (15.14)$$

Thus, θ_2 can be resolved as:

$$\theta_2 = \text{Atan2}(s_2, c_2) - (\pi/2 - 28.54^\circ) \quad (15.15)$$

To resolve θ_1 , for the both arms,

$$c_1 = \frac{{}^0_4P_{ex}}{L_1s_2} \quad (15.16)$$

$$s_1 = \frac{{}^0_4P_{ez}}{L_1s_2} \quad (15.17)$$

Thus, for the left arm,

$$\theta_1 = \text{Atan2}(s_1, c_1) - (\pi - 32.94^\circ) \quad (15.18)$$

For the right arm,

$$\theta_1 = \text{Atan2}(s_1, c_1) + 32.94^\circ \quad (15.19)$$

The transformation matrices 0_1T and 1_2T and their inverses ${}^0_1T^{-1}$ and ${}^1_2T^{-1}$ can be found accordingly.

Thus, the wrist position with respect to Frame 2, denoted ${}^2_7P_w = [{}^2_7P_{wx}, {}^2_7P_{wy}, {}^2_7P_{wz}]^T$, can be found:

$${}^2_7T = {}^1_2T^{-1} \cdot {}^0_1T^{-1} \cdot {}^0_7T = \begin{bmatrix} {}^2_7R & {}^2_7P_{wx} \\ {}^2_7P_{wy} \\ {}^2_7P_{wz} \\ 0 & 0 & 0 & 1 \end{bmatrix} \quad (15.20)$$

For the left arm,

$${}^2_7P_w = \begin{bmatrix} -L_2c_3s_4 \\ -L_1 - L_2c_4 \\ -L_2s_3s_4 \end{bmatrix} \quad (15.21)$$

For the right arm,

$${}^2_7P_w = \begin{bmatrix} -L_2c_3s_4 \\ -L_1 - L_2c_4 \\ L_2s_3s_4 \end{bmatrix} \quad (15.22)$$

To resolve θ_3 , for the both arms,

$$c_3 = \frac{{}^2_7P_{wx}}{-L_2s_4} \quad (15.23)$$

For the left arm,

$$s_3 = \frac{{}^2_7P_{wz}}{L_2s_4} \quad (15.24)$$

$$\theta_3 = \text{Atan2}(s_3, c_3) - (\pi - 53.6^\circ) - 2\pi \quad (15.25)$$

For the right arm,

$$s_3 = \frac{{}^2_7P_{wz}}{-L_2s_4} \quad (15.26)$$

$$\theta_3 = \text{Atan2}(s_3, c_3) + (\pi + 53.6^\circ) \quad (15.27)$$

The transformation matrix 2_3T and its inverse ${}^2_3T^{-1}$ can be found accordingly.

θ_5 , θ_6 and θ_7 can be derived from the transformation matrices from Frame 4 to Frame 7 4_7T .

$${}^4_7T = {}^3_4T^{-1} \cdot {}^2_3T^{-1} \cdot {}^1_2T^{-1} \cdot {}^0_1T^{-1} \cdot {}^0_7T = \begin{bmatrix} {}^4_7r_{11} & {}^4_7r_{12} & {}^4_7r_{13} & {}^4_7P_{wx} \\ {}^4_7r_{21} & {}^4_7r_{22} & {}^4_7r_{23} & {}^4_7P_{wy} \\ {}^4_7r_{31} & {}^4_7r_{32} & {}^4_7r_{33} & {}^4_7P_{wz} \\ 0 & 0 & 0 & 1 \end{bmatrix} \quad (15.28)$$

For the left arm,

$$\begin{aligned} {}^4_7T &= {}^3_4T^{-1} \cdot {}^2_3T^{-1} \cdot {}^1_2T^{-1} \cdot {}^0_1T^{-1} \cdot {}^0_7T \\ &= \begin{bmatrix} c_5c_6c_7 - s_5s_7 & -c_7s_5 - c_5c_6s_7 & c_5s_6 & 0 \\ -c_7s_6 & s_6s_7 & c_6 & L_2 \\ -c_5s_7 - c_6c_7s_5 & c_5c_7 - c_6s_5s_7 & -s_5s_6 & 0 \\ 0 & 0 & 0 & 1 \end{bmatrix} \end{aligned} \quad (15.29)$$

For the right arm,

$$\begin{aligned} {}^4_7T &= {}^3_4T^{-1} \cdot {}^2_3T^{-1} \cdot {}^1_2T^{-1} \cdot {}^0_1T^{-1} \cdot {}^0_7T \\ &= \begin{bmatrix} c_5c_6c_7 - s_5s_7 & -c_7s_5 - c_5c_6s_7 & c_5s_6 & 0 \\ c_7s_6 & -s_6s_7 & -c_6 & L_2 \\ c_5s_7 + c_6c_7s_5 & c_5c_7 - c_6s_5s_7 & s_5s_6 & 0 \\ 0 & 0 & 0 & 1 \end{bmatrix} \end{aligned} \quad (15.30)$$

Thus, for the left arm,

$$c_6 = {}^4_7r_{23} \quad (15.31)$$

$$s_6 = \sqrt{1 - c_6^2} \quad (15.32)$$

$$c_5 = \frac{{}^4_7r_{13}}{s_6} \quad (15.33)$$

$$s_5 = -\frac{{}^4_7r_{33}}{s_6} \quad (15.34)$$

$$c_7 = -\frac{{}^4_7r_{21}}{s_6} \quad (15.35)$$

$$s_7 = \frac{{}^4_7r_{22}}{s_6} \quad (15.36)$$

For the right arm,

$$c_6 = -\frac{4}{7}r_{23} \quad (15.37)$$

$$s_6 = \sqrt{1 - c_6^2} \quad (15.38)$$

$$c_5 = -\frac{4r_{13}}{s_6} \quad (15.39)$$

$$s_5 = -\frac{4r_{33}}{s_6} \quad (15.40)$$

$$c_7 = -\frac{4r_{21}}{s_6} \quad (15.41)$$

$$s_7 = -\frac{4r_{22}}{s_6} \quad (15.42)$$

For the left arm,

$$\theta_5 = \text{Atan2}(s_5, c_5) + \pi/2 \quad (15.43)$$

$$\theta_6 = \text{Atan2}(s_6, c_6) - \pi/2 \quad (15.44)$$

$$\theta_7 = \text{Atan2}(s_7, c_7) - \pi + 2\pi \quad (15.45)$$

For the right arm,

$$\theta_5 = \text{Atan2}(s_5, c_5) - \pi/2 \quad (15.46)$$

$$\theta_6 = \text{Atan2}(s_6, c_6) - \pi/2 \quad (15.47)$$

$$\theta_7 = \text{Atan2}(s_7, c_7) - \pi + 2\pi \quad (15.48)$$

For reaching movements, the four DOFs in consideration (three DOFs at the shoulder and one DOF at the elbow) can be resolved based on the wrist position P_w and the elbow position P_e : θ_4 is resolved according to Eq. (15.8); θ_1 , and θ_2 are resolved according to Eqs. (15.11)–(15.19). With regards to θ_3 ,

For the left arm,

$${}^2_5P_w = \begin{bmatrix} -L_2c_3s_4 \\ -L_1 - L_2c_4 \\ -L_2s_3s_4 \end{bmatrix} \quad (15.49)$$

for the right arm,

$${}^2_5P_w = \begin{bmatrix} -L_2c_3s_4 \\ -L_1 - L_2c_4 \\ L_2s_3s_4 \end{bmatrix} \quad (15.50)$$

Therefore, θ_3 can be resolved as Eqs. (15.23)–(15.27).

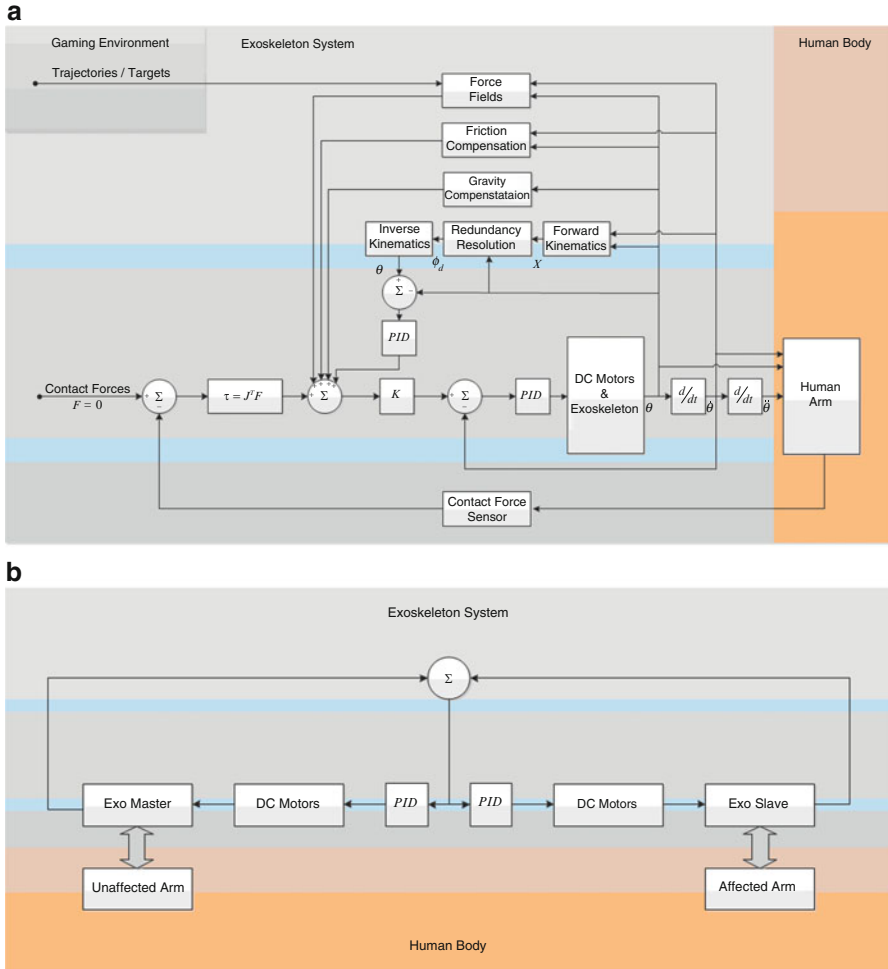


Fig. 15.5 A block Diagram of the exoskeleton control algorithms: (a) admittance control scheme – Single arm configuration, (b) teleoperation control scheme – dual arm configuration

15.2.3 Control Algorithms

15.2.3.1 Control Architecture of EXO-UL7: Overview

Two unique control algorithms are used to control the exoskeleton system in its unilateral (single arm) and bilateral (dual arm) modes of operation. The control modes guarantee that the system is inherently stable given the bandwidth of the human arm operation as the operators manipulate the system in virtual reality exposing the system to force fields and force feedback (haptic) effects (Fig. 15.5).

15.2.3.2 Admittance Control: Single Arm Exoskeleton

By definition, An admittance is the dynamic mapping from force to velocity. An admittance control scheme utilizes three multi-axis force/torque (F/T) sensors as the primary inputs. These F/T sensors are attached to all the physical interfaces between the operator's arm and the exoskeleton at the upper arm, forearm, and palm. A force applied on the exoskeleton system by the operator commands the exoskeleton arm to move with a velocity that is proportional to the force and along the same direction. As the force increases, the system responds by moving faster. This approach is also known as the "get out of the way" control scheme. As the system moves, the control scheme tries to set the interaction force to zero [34,35].

15.2.3.3 Teleoperation Control: Dual Arm Exoskeleton

In a teleoperation control scheme, the two arm exoskeleton system is configured as a master and a slave. The exoskeleton arm attached to the human unaffected (healthy) arm is defined as the master and the other exoskeleton arm attached to the affected (disabled) arm is defined as the slave. A local teleoperation scheme is used in which the master arm provides a position commands to the slave arm such that they both move in a mirror image fashion. Any joint angle generated by the unaffected arm is copied to the affected arm. In this mode of operation the unaffected arm controls the movements of the affected arm. The coupling between the arms will be varied. A tight coupling will be induced initially and it will be gradually reduced by 10 % in each treatment such that in the very last treatment, each arm will be completely independent (uncoupled).

15.2.3.4 Assistive Modes and Compensation Elements

The assistive modes are designed to further reduce the energy exchange between the human arm and the exoskeleton and to improve the transparency of human-robot interactions. Several force fields are applied on the patients as part on the training and their application and magnitude will be a function of the specific task.

Gravity Compensation Joint torques are generated in part due to the gravitational loads of the exoskeleton arm and the patient's arm. The gravity compensation algorithm estimates the joint torques for each arm configuration and provides a feed forward command to the actuators which in turn produce joint torques that counter the torque generated by gravity. This compensation will make the weight of the exoskeleton itself transparent to the operator. As such, the operator will feel as if the exoskeleton arm is completely weightless. This compensation mode will be active at all times. Furthermore, an identical algorithm will compensate for the gravitational loads of the patient's own arm such that the operator will not feel the weight of his/her arm. This compensation may vary between full compensation and

no compensation. The compensation of the patient's own arm will change during the treatment starting from full compensation during first treatment followed by a reduction of 10 % with each treatment that gradually exposes the patient to the full weight of the arm by the last day of the treatment.

Friction Compensation Friction is a force or a moment that resists the relative motion of the joints. The static/kinetic (coulomb) friction, as well as viscous friction is compensated through the feed forward element of the control algorithm such that the operator does not feel any resistance associated with friction.

Redundancy Resolution The human arm with its seven DOF (excluding scapular motion) is a redundant mechanism meaning that there are infinite arm configurations that can be adopted for the same position and orientation of the hand for grasping an object. Passing a virtual axis through the center of the shoulder joint and the center of the wrist joint allows us to define the position of the elbow joint by an angle defined with respect to this axis. This angle is defined as a swivel angle, which in turn defines in a parametric fashion the redundancy of the arm. Given the anatomical limitations of the shoulder and the wrist joint, the swivel angle has a specific range of angles from which any value to be selected will not change to the position or the orientation of the hand. The motor control system selects a specific swivel angle within the available range, and in that way resolves the arm redundancy. Since the human arm and the exoskeleton system are mechanically coupled, the redundancy resolution imposed by the exoskeleton system has to match the same solution that would have been adopted by a neuromuscular system. The algorithm implemented into the exoskeleton is based on an extensive preliminary study of this problem with both healthy and stroke patients. This algorithm synthesizes three classes of criteria: (1) kinematic criteria, (2) dynamic criteria, and (3) comfort criteria. The weight factors of each one of the three criteria change dynamically and will predict the swivel angle for the next time interval. One should note that the redundancy resolution is only required in the unilateral mode of operation. During the bilateral mode of operation, the swivel angle of the unaffected arm is transmitted to the affected arm, thus the exoskeleton system adopts the motor control redundancy resolution.

15.2.4 Redundancy Resolution

The redundancy resolution is critical in the control of the exoskeleton, in order to achieve the transparency of the interaction between the exoskeleton and its operator. Ideally, the redundancy resolution controls the exoskeleton in the same way that the human motor system controls arm movements. Therefore, the exoskeleton can be used for power augmentation for the healthy human arm movements, as well as for the correction of the abnormal arm movements in stroke rehabilitation.

The problem of controlling redundant degrees of freedom, i.e., redundancy resolution, has been previously considered in the control of robot manipulators. When solving an inverse kinematics or dynamics problem for manipulation tasks, redundant degrees of freedom can be used to achieve secondary goals such as to satisfy certain task constraints or to improve task performances. Task-based redundancy resolutions control the extra DOF by integrating the task-dependent constraints into an augmented Jacobian matrix [36, 37]. Performance-based redundancy resolutions may optimize the manipulability [19, 38–40], energy consumption [41, 42], the smoothness of movement [43–46], task accuracy [47] and control complexity [48].

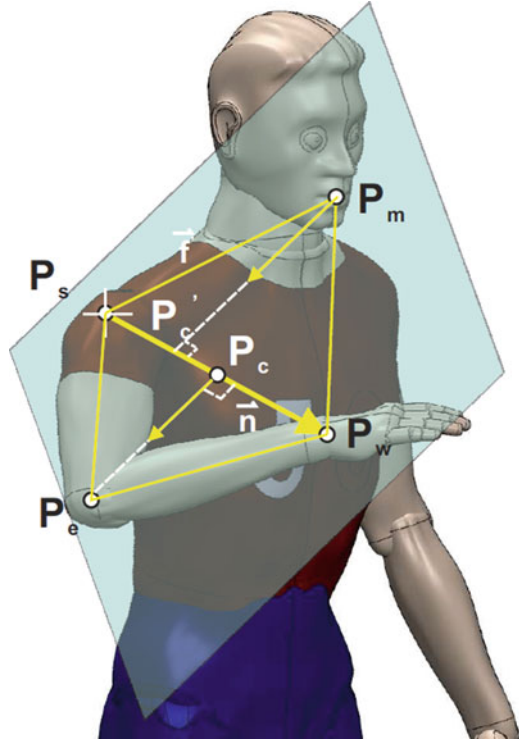
The EXO-UL7 exoskeleton is designed to assist the operator's arm movements in unexpected tasks and in uncertain environments. It requires a real-time control rather than a pre-planned motion control, and the redundancy resolutions have to be based on local (instead of global) performance optimization. Under the above constraints, we investigate the study of the motor control of the human arm movements and select several control criteria, which are applicable for the control of the exoskeleton. The selected criteria optimize different performances in motion control, including motion efficiency, motion smoothness, energy consumption and etc.

15.2.4.1 Maximizing the Motion Efficiency

H. Kim *et al.* proposed a redundancy resolution that determines the swivel angle by maximizing the motion efficiency [19]. As shown in Fig. 15.6, when the elbow falls on the plane formed by the positions of the shoulder P_s , the wrist P_w and the virtual target P_m , the projection of the longest principle eigen-vector of the manipulability ellipsoid on the direction from the hand to the virtual target P_m is maximized, and so is the motion efficiency towards the virtual target P_m , which is hypothesized to be on the head. Given the role of the head as a cluster of sensing organs and the importance of arm manipulation to deliver food to the mouth, it is hypothesized that the swivel angle is determined by the human motor control system to efficiently retract the hand to the head region.

A good candidate for the position of virtual target is the position of the mouth. This hypothesis is supported by intracortical stimulation experiments that evoked coordinated forelimb movements in conscious primates [49, 50]. It has been reported that each stimulation site produced a stereotyped posture in which the arm moved to the same final position regardless of its posture in the initial stimulation. In the most complex example, a monkey formed a frozen pose with its hand in a grasping position in front of its open mouth. This implies that during the arm movement toward an actual target, the virtual target point at the head can be set for the potential retraction of the palm to the virtual target.

Fig. 15.6 The proposed redundancy resolution intends to maximize the motion efficiency by maximizing the projection of the longest principle eigen-vector of the manipulability ellipsoid on the direction from the hand to the virtual target P_m . The corresponding elbow position falls on the plane formed by P_s , P_w and P_m



15.2.4.2 Minimizing Work in the Joint Space

Minimizing work in the joint space is proposed by T. Kang as a real-time dynamic control criterion, which resolves the inverse kinematics by minimizing the magnitude of total work done by joint torques for each time step [42]. With the dynamic arm model, the joint torques (T) can be extracted given the states of the arm. The calculation of work in the joint space for each time step depends on (1) the joint torques and (2) the difference in joint angles. Therefore, the work in the joint space during the movement interval $[t_k, t_{k+1}]$ can be computed for two different conditions. The dynamic constraint adopted in this chapter is from the original work done by the aerospace medical research laboratory [51]. Here, we briefly include the essential parts of the algorithm for the integrity of the chapter:

$$\text{if } T_{i,t_k} \cdot T_{i,t_{k+1}} > 0,$$

$$W_i = \frac{(T_{i,t_k} + T_{i,t_{k+1}}) \cdot \Delta q_i}{2} \tag{15.51}$$

where T_{i,t_k} and $T_{i,t_{k+1}}$ are the joint torques of the i -th joint at the time t_k and t_{k+1} . $\Delta q_i = (q_{i,t_{k+1}} - q_{i,t_k})$ is the difference of the i -th joint angle during the time interval $[t_k, t_{k+1}]$.

When $T_{i,t_k} \cdot T_{i,t_{k+1}} < 0$,

$$W_i = \frac{(|\Delta q_i| - h_i) \cdot T_{i,t_{k+1}}}{2} - \frac{h_i \cdot T_{i,t_k}}{2} \quad (15.52)$$

where $h_i = (|T_{i,t_k}| \cdot |\Delta q_i|) / |T_{i,t_{k+1}} - T_{i,t_k}|$ and denotes the difference of the i -th joint angle from q_{i,t_k} to the value corresponding to the zero crossing of joint torque.

To minimize the work done in the joint space at each time step (e.g. $|W|_{t_k,t_{k+1}}$ for the time interval $[t_k, t_{k+1}]$), the swivel angle of the arm for a specified wrist position is optimized by:

$$\begin{aligned} \phi(k+1) &= \arg \min_{\phi'(k+1)} |W_i|_{t_k,t_{k+1}} \\ &= \arg \min_{\phi'(k+1)} \sum_{i=1}^4 |W_i|_{t_k,t_{k+1}} \end{aligned} \quad (15.53)$$

where $|W_i|_{t_k,t_{k+1}}$ denotes the work done by the i -th joint.

15.2.4.3 Minimizing Joint Angle Change

Minimizing joint angle change is a real-time kinematic criterion that impose smooth motion in the joint space. Given the expected positions of the wrist $P_w(k+1)$ and the shoulder $P_s(k+1)$, this criterion explores the possible the swivel angles for the next time step $\phi'(k+1)$ and selects the one which minimizes the norm of the change in the joint angle vector. For daily activities, the change in swivel angle within 0.01 s is supposed to be no larger that 0.5° . Given the current swivel angle $\phi(k)$, we search within the range of $[\phi(k) - 0.5, \phi(k) + 0.5]^\circ$ by the step of $\delta\phi = 0.1^\circ$. The swivel angle for the next time step $\phi(k+1)$ is determined by:

$$\begin{aligned} \phi(k+1) &= \arg \min_{\phi'(k+1)} |\theta(k) - \theta'(k+1)| \\ &= \arg \min_{\phi'(k+1)} \sqrt{\sum_{i=1}^4 (\theta_i(k) - \theta'_i(k+1))^2} \end{aligned} \quad (15.54)$$

In Eq. (15.54), $\theta(k) = [\theta_1(k), \theta_2(k), \theta_3(k), \theta_4(k)]^T$ is the joint angle vector for current time step. $\theta'(k+1)$ is the joint angle vector for the next time step computed from a possible $\phi'(k+1)$ value.

At the kinematic level, alternative control criteria can optimize motion smoothness by minimizing jerk (the square of the first derivative of acceleration) in the joint space and/or task space, to account for the straight paths and bell-shaped speed profiles observed in reaching movements [43, 44, 52]. At the dynamic level, the

optimization of smoothness can be achieved by minimizing the change in joint torque [45, 46], which explains the mild curvature in the roughly straight hand-reaching trajectories in the task space. By observing various implementations, we have noticed that minimizing the norm of the change in the joint angle performs better than minimizing the norm of the change in higher order derivatives of the joint angle (e.g., velocity and acceleration). These control strategies are for global motion planning and the computation of the trajectories in the task space and/or the joint space before execution. Since the exoskeleton is designed to move with the operator in unexpected task and uncertain environment, the smoothness of motion is expected to be addressed more locally than globally.

15.2.4.4 Minimizing the Change in Kinetic Energy

Minimizing the change in kinetic energy is based on the following hypothesis: since human movements are well adapted to gravity, unless the dynamics of the human body is significantly affected by additional load, the motor control system may plan the movements at daily-activity speed without compensating much for gravity. With the dynamic model, the kinetic energy (Ke) can be computed given the state of the arm. Similar to Criterion 3, we explore the possible swivel angles for the next time step and find the one that minimizes the change in the kinematic energy.

$$\phi(k+1) = \arg \min_{\phi'(k+1)} |Ke(k) - Ke'(k+1)| \quad (15.55)$$

For global energy optimization, J.F. Soechting *et al.* minimize the peak value of kinetic energy, which requires the knowledge of the final arm posture [41]. In addition, A. Biess *et al.* integrate the consideration of kinetic energy in the control strategy by looking for a geodesic path in the Riemannian configuration space, which consumes less muscular effort since the sum of all configuration-speed-dependent torques vanishes along the path [53]. For the real-time control of the exoskeleton, we prefer minimizing the change in kinetic energy locally.

15.2.5 Performance Comparison of Different Redundancy Resolutions

To study the performance of different redundancy resolutions, we collect data of the point-to-point reaching movements in a 3D workspace from healthy subjects (see Figs. 15.7 and 15.8). The arm postures predicted by different redundancy resolutions are compared and evaluated with reference to the measured arm postures.

A comparison of the arm posture prediction performance has been conducted between the redundancy resolutions by maximizing motion efficiency (Redundancy Resolution I) and by minimizing work in the joint space (Redundancy Resolution II). The mean (μ) and standard deviation (σ) of the prediction errors are

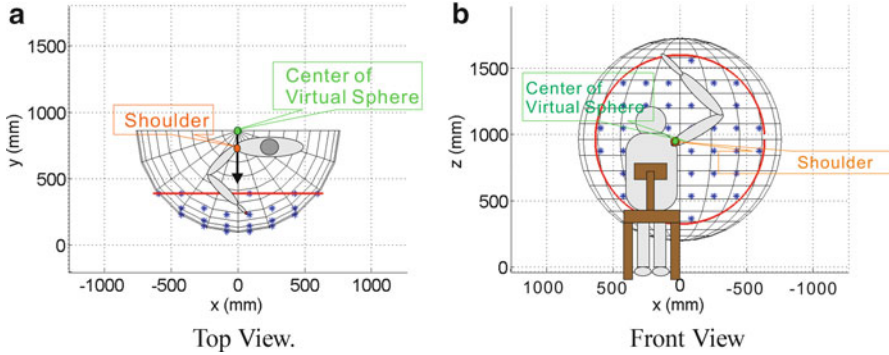


Fig. 15.7 The spherical workspace for the reaching movement experiments: (a) the top view and (b) the front view. The height of the workspace center is adjustable and is always aligned with the right shoulder of the subject

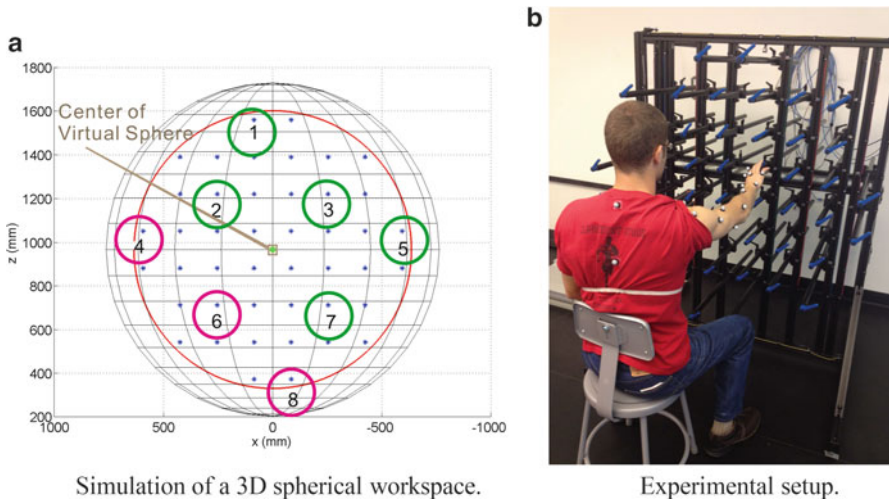


Fig. 15.8 (a) Eight targets are selected among all the available targets (denotes as blue dots) in the spherical workspace. Considering the motion range of the right arm, Target 1, 2, 3, 5, 7 (in green circles) are within the comfortable arm motion range, while Target 4, 6, and 8 (in magenta circles) are close to the motion range boundary. (b) A subject is performing the instructed reaching movement. The subject is seated in a chair with a straight back support. The right arm is free for reaching movements, while the body of the subject is bounded back to the chair to minimize shoulder displacement. During the experiment, the subject uses index finger to point from one instructed target to another, with his/her wrist kept straight. A motion capture system catches the positions of the passive-reflective markers attached to the torso and the right arm, recording the movements at 100 Hz

computed for each individual valid trail (2,674 out of 2,800 in total), and their distributions are presented in Fig. 15.9. It is shown that the Redundancy Resolution II has higher performance on both the mean and standard deviation of the prediction errors, which results from the fact that Redundancy Resolution II has to start its prediction from the arm posture measured at the beginning of the movement, while Redundancy Resolution I does not need to initialize its prediction with any measured data. One way to improve the performance of Redundancy Resolution I is to estimate the position of the virtual target dynamically based on the recent history of the swivel angle measurements. As shown in Fig. 15.9e,f, the improved performance is slightly higher than that of Redundancy Resolution II [54].

15.3 Clinical Study: Application of EXO-UL7 on Stroke Rehabilitation

15.3.1 *Experiment Protocols*

15.3.1.1 Apparatus

The system used for this research consisted of the upper limb exoskeleton EXO-UL7, a control computer, and a game computer. The control computer used PID control to provide gravity compensation, as well as bilateral symmetric assistance or unilateral assistance, as needed. In all cases where assistance was provided, the robot only provided partial assistance, helping subjects by giving a helpful push in the desired direction [6, 7, 55].

The games were created using Microsoft Robotic Developer Studio [56]. The game computer was connected to a 50" flat screen monitor. In addition to generating real time virtual reality [57] game images, the game computer also collected position and force data at 100 Hz.

The games are depicted in Fig. 15.10. The games were played for 10–15 min each. Over the course of the study, each subject played every game multiple times. Therefore, the rehabilitative efficacy of any given game is confounded with the other games [58]. The BSRMT group played each game using both arms and the URMT group played each game using only the paretic arm. For BSRMT, the subject's less-affected arm was the master, and the paretic arm was the slave. As subjects moved their less-affected arm the robot moved the paretic arm in a mirror-image fashion. Aside from gravity compensation, for URMT, the robot only provided partial assistance in the Flower game (see Fig. 15.1a). A more detailed evaluation of these games is provided in [6].

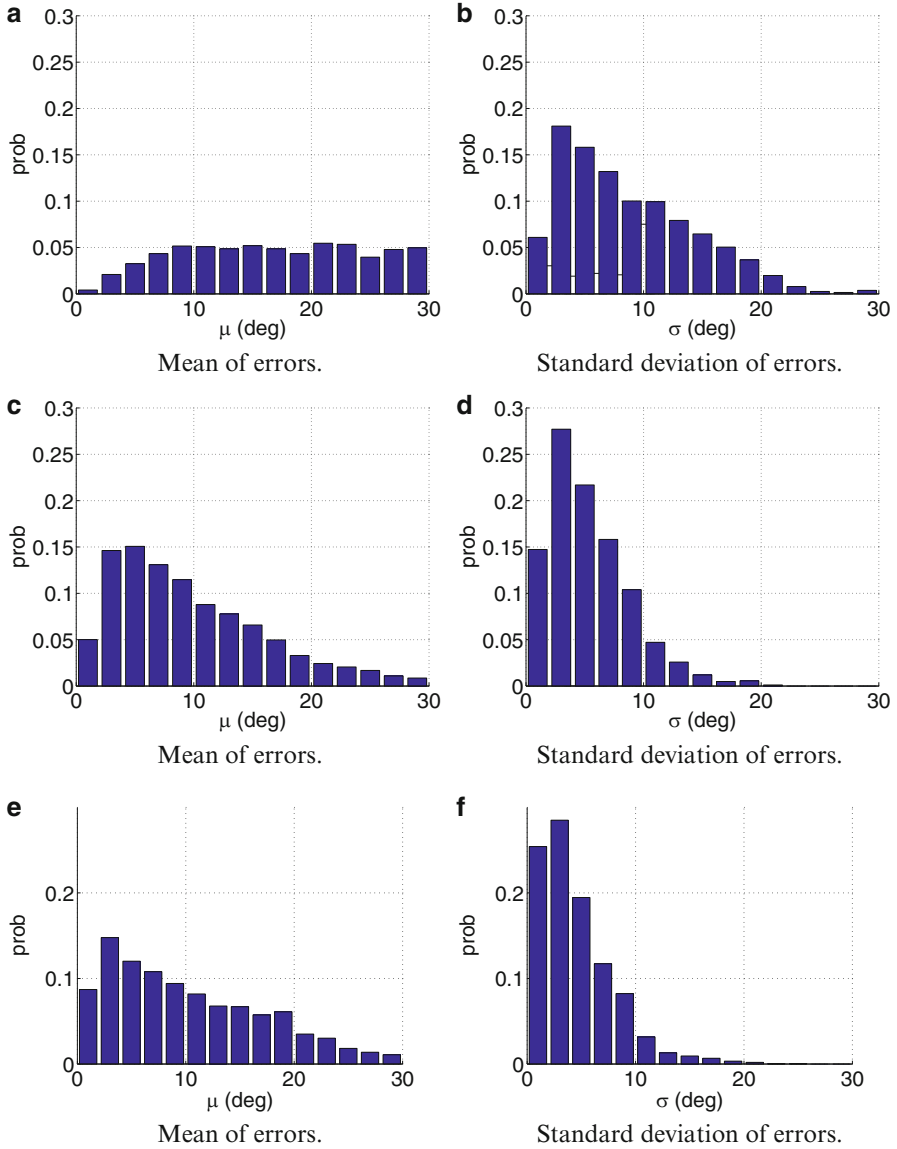


Fig. 15.9 Swivel angle prediction performance of the redundancy resolutions by maximizing the motion efficiency (the Redundancy Resolution I, see (a) and (b)) and by minimizing the work in joint space (the Redundancy Resolution II, see (c) and (d)). The performance of Redundancy Resolution I can be improved by dynamic estimation of the position of the virtual target (see (e) and (f))

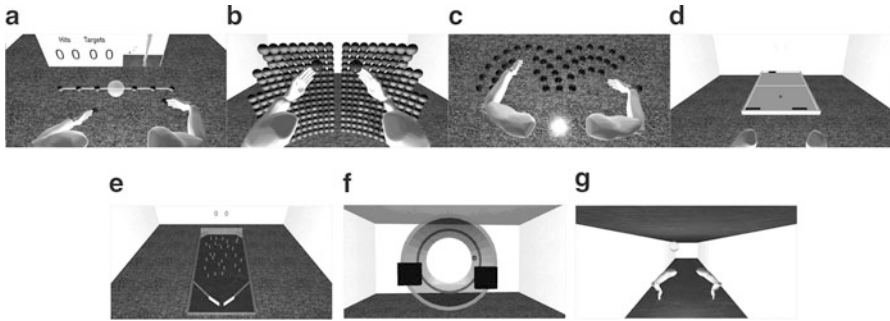


Fig. 15.10 Screen shots from the various games. The avatar arms move in response to the movement of the subject. In the Pinball and Circle games, avatar arms are not visible so that the view of the Pingpong table will not be blocked. (a) Flower game. (b) Paint game. (c) Reach game. (d) Pong game. (e) Pinball game. (f) Circle game. (g) Handball game

15.3.1.2 Pilot Study

Ten male and female subjects between 27 and 70 years of age, for more than 6 months post stroke, with a Fugl-Meyer score between 16 and 39 and a score of 19 or greater on the VA Mini Mental Status Exam were recruited for the study. All were screened and consented prior to a random assignment. The subjects were sub-categorized by severity and then randomly assigned to either the unilateral robotic training or to the bilateral robotic training. All subjects were scheduled for 12 training sessions. The visits were scheduled twice a week for 6 weeks. This study was approved by the Committee on Human Research at the University of California-San Francisco (UCSF) and each session was performed at UCSF under the guidance of a trained therapist.

In the pilot study, subjects sit in front of a screen with a virtual reality game to play. In this game, small target balls are located spherically around the robot. When the target balls with the tip of the virtual arm is touched, the ball color changes (see Fig. 15.11). The ratio of the touched balls to the total number of target balls can be used to assess the mobility improvement of the subjects.

15.3.1.3 Unilateral and Bilateral Robotic Training via the EXO-UL7

The research on the unilateral and bilateral robotic training was approved by the University of California, San Francisco, Committee on Human Research. Interventions consisted of 12, 90-min sessions of robotic assisted training or standard care. An elastic restraint around the torso and thighs helped subjects maintain a neutral sitting position during robotic training. The experimental setup is depicted in Fig. 15.12.

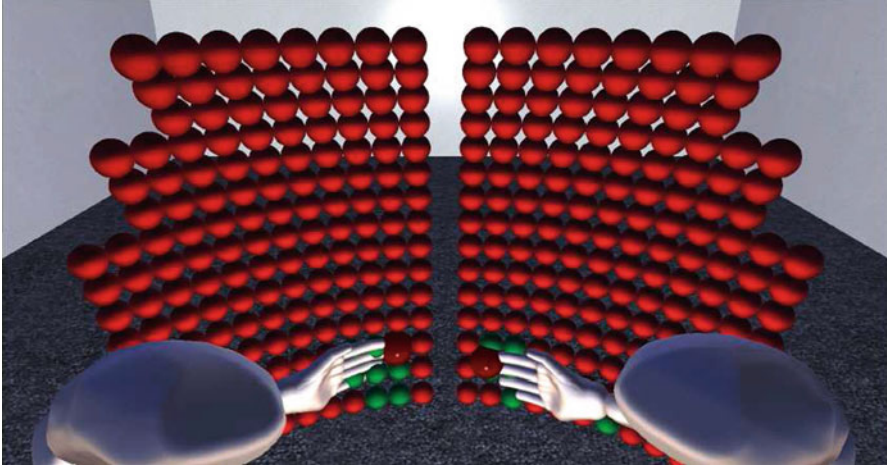


Fig. 15.11 Pilot study: Subjects paint the virtual environment in either a unilateral control or bilateral control architecture



Fig. 15.12 A subject with right-side hemiparetic performing BSRMT

Included were 15 subjects who are more than 6 months post stroke, ranging in ages from 23 to 69 years, with Fugl-Meyer scores between 16 and 39. The subjects were stratified by their Fugl-Meyer score and then randomly assigned to the

BSRMT, URMT or usual care with a physical therapist. With an upper limb Fugl-Meyer score between 16 and 39, each subject had the necessary control of their paretic arm to be able to play the games, while still having the potential for improvement.

Improvement Metrics This work includes just a fraction of clinical measures that were gathered from this study. The measures considered presently include: spasticity, dexterity, hand strength, and shoulder range of motion (ROM). These measures all assess different aspects of motor dysfunction. In that sense, they are independent. The reason for focusing on these measures is because they were explainable using kinematic analysis. For example, it is difficult to relate kinematic analysis to measures such as psychological state or pain scales. Additionally, these metrics all involved data that suggested a significant change in performance as measured before and after the intervention.

Data Analysis Clinical data was analyzed using standard hypothesis testing. Specifically, for each test type, the corresponding subject groups were tested for a significant change in performance as measured before and after the intervention. This includes paired t-tests for parametric measures and 2-Sample Wilcoxon-Mann-Whitney (Wilcoxon) tests for non-parametric data. For both types of tests, p-values were reported. For the Wilcoxon test, p-values were adjusted for ties where applicable. Statistical calculations were performed using Minitab Statistical Software (Minitab Inc., State College, PA, USA). Confidence limits of 95 % ($p < 0.05$) and 90 % ($p < 0.01$) were used to test significance. A confidence limit of 90 % is generally not used for clinical assessments [59,60]. However, 90 % limits are used in other contexts, albeit as a lower limit. Given the comparatively small population of subjects in each training group ($n = 5$), this study is best described as a pilot, or feasibility study. Notwithstanding, only relatively large differences will achieve the 95 % level for sample sizes such as this and it is left to the discretion of the reader how to interpret these levels.

Over the past decades, a large number of metrics have been proposed to assess human movements using robots and/or motion capture [55]. There are two difficulties with such approaches. First, it is often unclear if a change in a given metric is caused by legitimate rehabilitation or if it is related to familiarity with the system. For example, a subject might improve at playing a given game even though there is no actual therapeutic improvement. Second, real-time, multi-joint force and velocity data are generally not available in clinical settings, nor are they standardized. Therefore, measures that are gathered from a given robotic system are difficult to replicate. It is also unlikely that they directly translate to standard clinical measures. For these reasons, this research focused on clinical measures of performance that were collected before and after the intervention. Kinematic data collected from the robot were used to contrast movement training differences

between BSRMT and URMT modes, but not as a measure of improvement. For a detailed analysis of subject performance using kinematic data collected from the robot, see [16].

The Data Analysis Section references joints by number. The directions of positive joint rotation are depicted in Fig. 15.2. In words, the axes are defined as follows: Joint 1 is a combination of shoulder flexion and abduction; Joint 2 is a combination of shoulder flexion and adduction; Joint 3 shoulder inner rotation, Joint 4, elbow flexion; Joint 5 is the elbow/wrist supination; Joint 6 is the wrist flexion; and joint 7 is the wrist ulnar deviation.

In an effort to tie the clinical outcomes to training, a metric is needed to quantify overall movement training. A long-standing tenet in the rehabilitation community is that repetition of movement is required for recovery. To quantify overall movement training for a given game during a given trial, seven numbers are calculated, one for each joint. Each of the seven numbers relate to the proportional contribution of movement for a given joint. An eighth number is calculated to capture the overall intensity of movement. With respect to the proportions of movement for each of the seven joints, a row vector is defined as Eq. (15.56):

$$|p_1 \ p_2 \ p_3 \ p_4 \ p_5 \ p_6 \ p_7| \quad (15.56)$$

where p_1 is the proportion of rotation for joint 1, p_2 is the proportion of rotation of joint 2, and so on. Accordingly,

$$|\sum_{i=1}^7 p_i = 1| \quad (15.57)$$

Thus, the sum of the proportions account for 100 % of the total joint rotation for the 7 DOF of the arm. The 8th number being calculated is the “intensity” of the training and is given by I . Thus, the intensity of training for joint j is given by $p_j \dot{I}$.

Equations (15.56) to (15.57) require some measure of movement training intensity. One approach is to calculate the total angular position, velocity, and acceleration for a given joint. As a start, consider the angular position. A change in the angular position is given as $\Delta\theta$. Summing $\Delta\theta$ for successive samples in the data set is infeasible because rotations in one direction will be canceled with rotations in the other direction. Therefore, a more suitable calculation for the angular position of the j -th joint is to take the RMS as follows:

$$\mathbf{RMS}_{\theta_j} = \sqrt{\frac{1}{n} \sum_{i=1}^n \Delta\theta_{i,j}} \quad (15.58)$$

where n is the number of joint measurements, and i is the i th measurement. Angular velocity, ω is given by $\Delta\theta/\Delta t$. Therefore, the RMS for ω is given by

$$\mathbf{RMS}_{\theta_{\omega,j}} = \sqrt{\frac{1}{n} \sum_{i=1}^n \left(\frac{\Delta\theta_{i,j}}{T_s} \right)^2} \quad (15.59)$$

where T_s is the sample time. In this case, the sampling rate was 100 Hz and $T_s = 0.01$ s. Because T_s is a constant, Eq. (15.58) is essentially the same calculation Eq. (15.59) except that it is scaled by the constant value $1/T_s$. Therefore, calculating the RMS of both angular position and angular velocity is of little value and the discussion that follows considers only angular velocity and acceleration.

In an effort to minimize the effects of noise and finite sampling times, a 5-point numerical differentiation was used to calculate the RMS for angular velocity and acceleration. Thus, the RMS calculation that is used for velocity is

$$\mathbf{RMS}_{\theta_{\omega,j}} = \sqrt{\frac{1}{n} \sum_{i=1}^n \left(\frac{-\theta_{i+2,j} + 8\theta_{i+1,j} - 8\theta_{i-1,j} + \theta_{i-2,j}}{12T_s} \right)^2} \quad (15.60)$$

and for angular acceleration,

$$\mathbf{RMS}_{\theta_{a,j}} = \sqrt{\frac{1}{n} \sum_{i=1}^n \left(\frac{-\theta_{i+2,j} + 16\theta_{i+1,j} - 30\theta_{i,j} + 16\theta_{i-1,j} - \theta_{i-2,j}}{12T_s} \right)^2} \quad (15.61)$$

With the RMS calculations for angular acceleration and velocity in hand, calculating the proportional contributions of each joint according to Eq. (15.56) is obtained by the following equation:

$$\left(\sum_{j=1}^n RMS_j \right)^{-1} |RMS_1 \ RMS_2 \ RMS_3 \ RMS_4 \ RMS_5 \ RMS_6 \ RMS_7| \quad (15.62)$$

The proportions given in Eq. (15.62) are presented as percentages throughout this chapter. Intensity I is calculated for each game of each trial for both angular acceleration and angular velocity using the average RMS of the 7 joints. The intensity calculation is given as follows:

$$I = \frac{1}{7} \sum_{j=1}^7 RMS_j \quad (15.63)$$

Data processing was accomplished using custom MatlabTM scripts (The Mathworks Inc, Natick, MA, USA).

15.3.2 Results

15.3.2.1 Pilot Study

During the clinical trial for the paint game, the travel distance and time-to-finish were recorded. Averaged travel distances show that the bilateral training group traveled 2.2 m/session and unilateral group did 1 m/session. The bilateral group spent 22 s/session and unilateral group spent 12 s/session. The percent improvement defined between the first and last session 12 weeks later showed that the bilateral and unilateral training group had 97 and 2 % improvement, respectively for the travel distance, while both groups showed similar improvement for time-to-finish [16].

15.3.2.2 Clinical Outcomes of the Unilateral and Bilateral Robotic Training

Clinical Measures Non-parametric data are summarized in Figs. 15.13–15.16 and parametric data are summarized in Figs. 15.17–15.19. For each group the average percent change is calculated for parametric data. For non-parametric data the median change is calculated. Also, a p-value for the corresponding hypothesis test (Wilcoxon or paired-t test) is given below each plot. The bold type indicates significant differences. The strongest changes, $\alpha \leq 0.05$, are distinguished with a dark shade of box plot gray for parametric data. For $0.05 < \alpha \leq 0.10$, the box plots are distinguished with a lighter shade of gray.

There was a statistically significant reduction in finger flexion (see Fig. 15.13b), and elbow flexion/extension spasticity for URMT, see Fig. 15.13c, d, as well as a significant improvement on the Box and Block Test (see Fig. 15.17b). However, there was a significant reduction in grip strength for URMT, as measured with a Jamar hand dynamometer (Lafayette Instrument Company, Lafayette, IN).

There were significant differences for ROM [61] in the shoulder for all three groups, see Fig. 15.18e–g. All ROM measurements were performed with a goniometer. There was a relatively large improvement in shoulder abduction for the BSRMT, see Fig. 15.18e, and the standard care groups. The subjects in the BSRMT group also had significant improvements for shoulder external rotation ROM, see Fig. 15.18g. The URMT group had the least improvement in shoulder ROM. In addition, the BSMRT group had a significant reduction in internal rotation ROM at the shoulder, see Fig. 15.18f.

Movement Training Measures At times subjects would pause their movement training. Causes for such halting could result from a variety of reasons. Examples include: stops for technical corrections for the robot or game, readjustments of straps or restraints, dialog with the subjects, respites, and bathroom breaks. As a specific example, a training interval of approximately 300 s is depicted in Fig. 15.20.

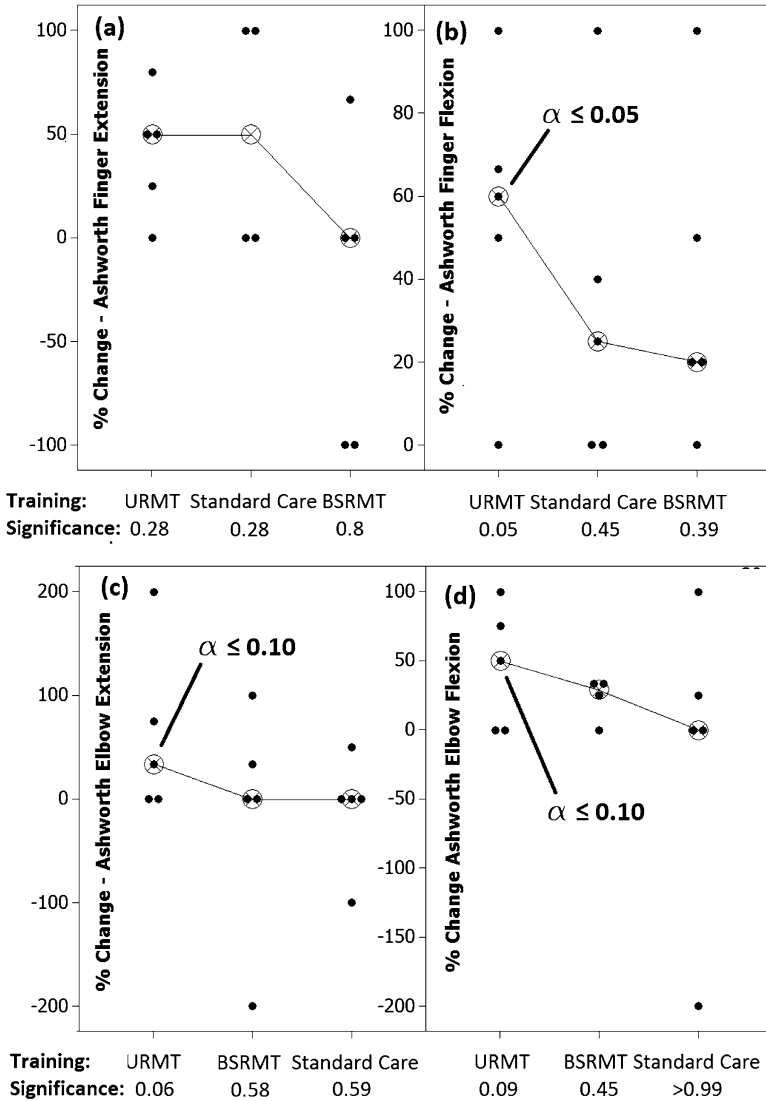


Fig. 15.13 Individual value plots of clinical measures for non-parametric data: **spasticity metrics**. Individual values represent percent improvements as measured before and after the intervention. Also depicted are significant ($p \leq 0.05$), or marginally significant ($p \leq 0.10$) changes as determined by a Wilcoxon test. Connecting lines attach median values. Note, for cases where a decrease in a metric is regarded as an improvement the individual values are given positive, and vice-a-versa

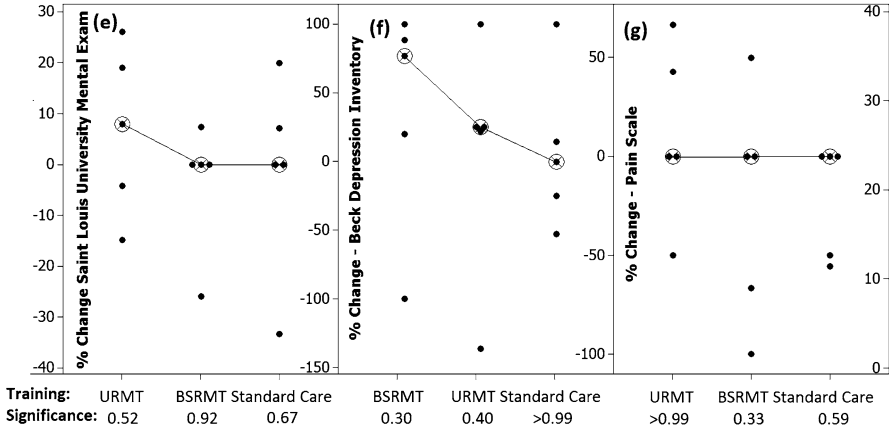


Fig. 15.14 Continue Fig. 15.13. Individual value plots of clinical measures for non-parametric data: **psychological metrics**

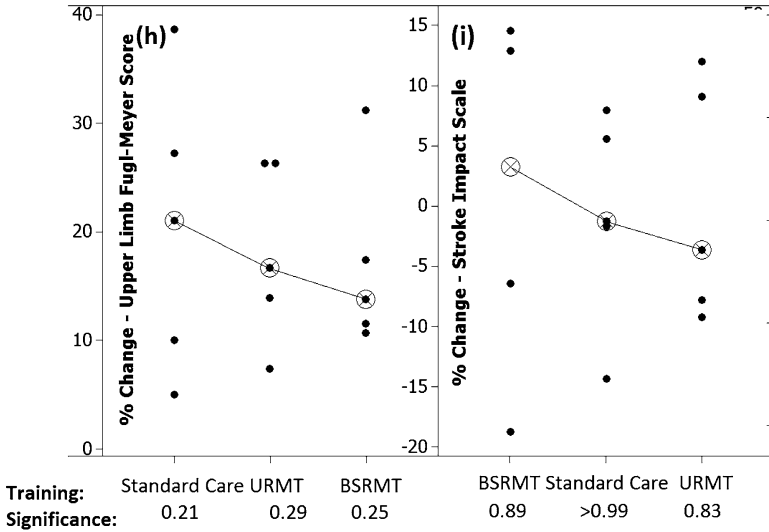


Fig. 15.15 Continue Fig. 15.14. Individual value plots of clinical measures for non-parametric data: **general metrics**

Notice that there are two apparent pauses wherein most of the joints stop moving (flat lines). Pauses such as this will deflate the measures given by Eq. (15.60) and Eq. (15.61). Perhaps the most accurate measure of training intensity Eq. (15.63) and percent contributions Eq. (15.62) would consider only data with the pauses removed. However, such segregation of data is open to interpretation and is fought with uncertainty. For this reason, the following analysis will consider data sets only for the top 50-th percentile of training as measured by intensity. Cases where training is

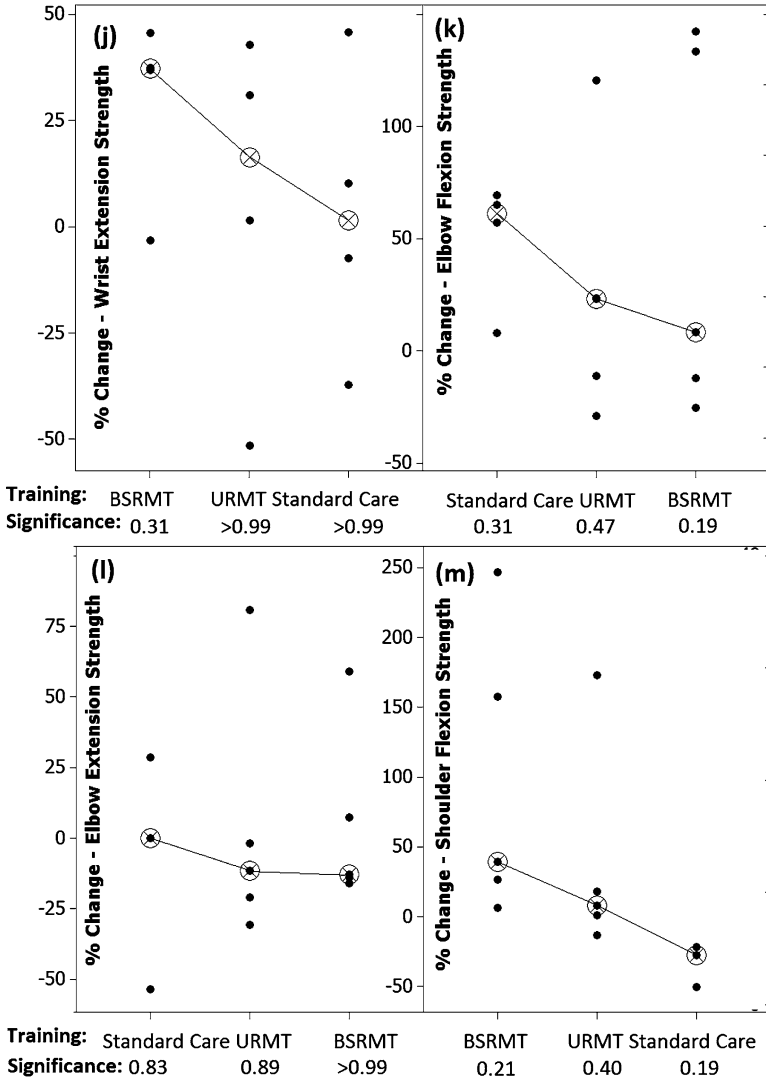


Fig. 15.16 Continue Fig. 15.15. Individual value plots of clinical measures for non-parametric data: **strength metrics**

halted will result in lower intensities. Therefore, by excluding the lower half of the data, it is more assured that data analysis only includes training that was continuous and without interruption.

Figure 15.23 depicts URMT percentage contributions by joint for velocity Eq.(15.60) and acceleration Eq.(15.61). Each element in Eq.(15.62) is summarized statistically as a CI for velocity and acceleration. Notice that angular

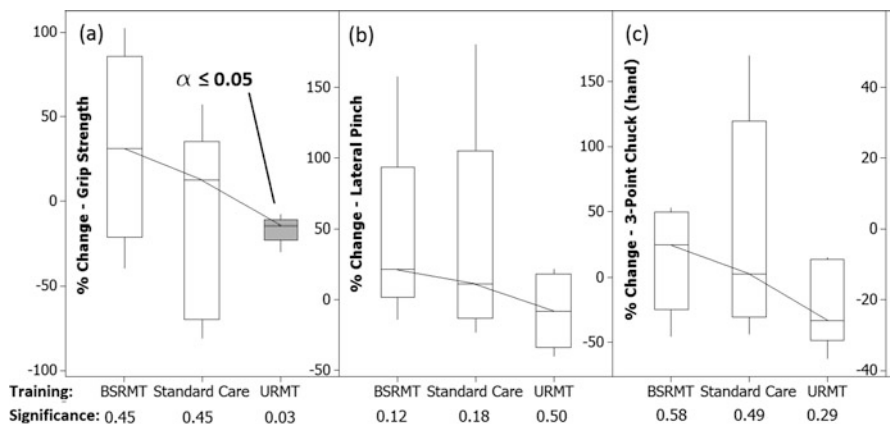


Fig. 15.17 Box plots of clinical measures for parametric data: **hand strength metrics**. Individual values represent percent improvements as measured before and after the intervention. Also depicted are significant ($p \leq 0.05$), or marginally significant ($p \leq 0.10$) changes as determined by a paired t-test. Connecting lines attach mean values

velocity and acceleration track are fairly close for each joint. In general, based on the percent contributions of each joint, and the training intensities, velocity and acceleration tended to co-vary. Putting it in another way, comparison of BSRMT and URMT by velocity was roughly equivalent to using acceleration. Therefore, considering the differences between BSRMT and URMT in terms of velocity and acceleration are of little value. Thus, with the proviso that acceleration would have been an equally valid measure, the remainder of this chapter will consider only velocity RMS values.

Depicted in Fig. 15.21 is a comparison of the affected arm to the control arm for BSRMT. Perhaps not surprisingly, the control arm had similar joint contribution percentages as the affected hemiparetic arm. However, in terms of intensity, the affected was significantly lower than the control arm, $p = 0.017$, see “All joints” in Fig. 15.22.

Bilateral Symmetric Versus Unilateral Training Because the improvement of the affected side is most important, the following comparison between BSRMT and URMT considers only the paretic arms. This comparison is summarized in Fig. 15.23. The most important difference was in terms of intensity. The right most set of CI’s in Fig. 15.9 depicts the overall intensity of bilateral versus unilateral training as calculated by Eq. (15.63). A 2-sample t-test indicated that there was a statistically significant difference in intensity between the two training groups ($p - value < 0.001$) with BSRMT having a mean intensity that was 25 % higher than URMT. Additionally, Fig. 15.23 shows that the BSRMT resulted in a higher proportion of movement for Joint 4 (elbow). Thus, the EXO-UL7 imposed significantly higher velocities on the wrist and elbow as it attempted to maintain symmetry between the paretic arm and the faster moving unaffected arm.

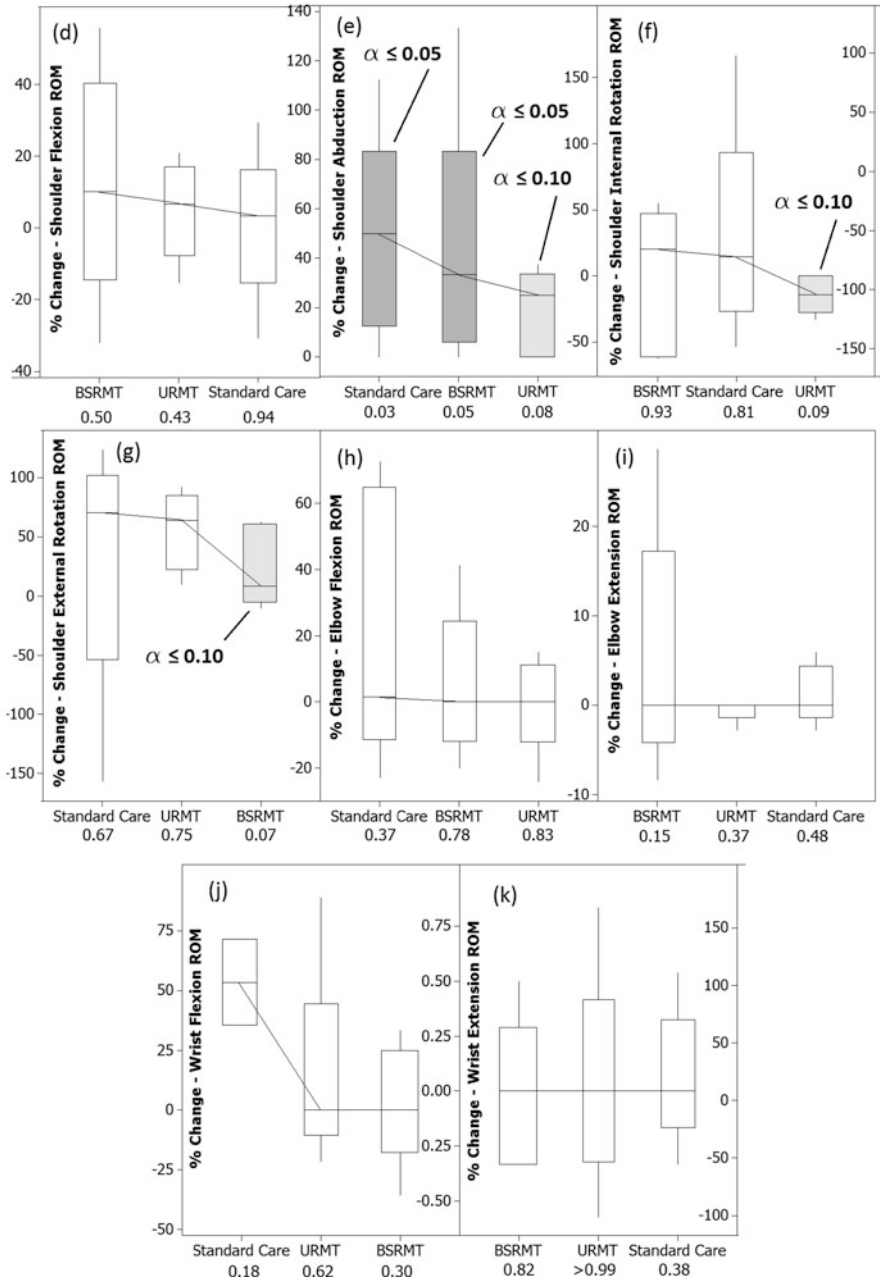


Fig. 15.18 Continue Fig. 15.17. Box plots of clinical measures for parametric data: **range of motion metrics**

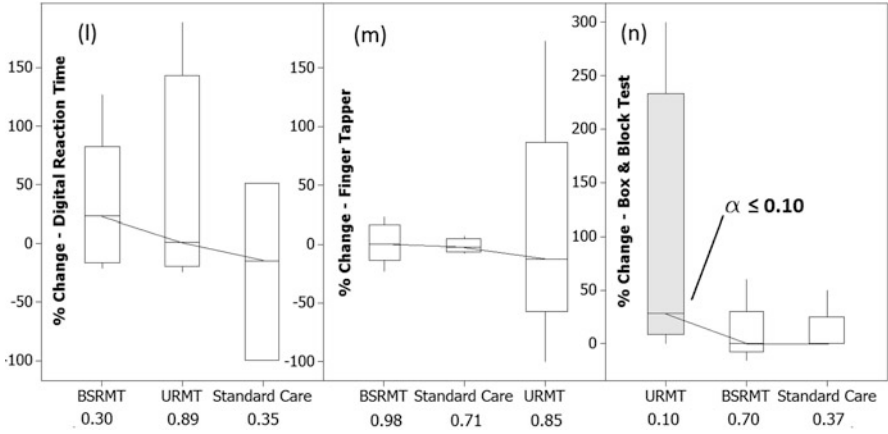


Fig. 15.19 Continue Fig. 15.18. Box plots of clinical measures for parametric data: **dexterity metrics**

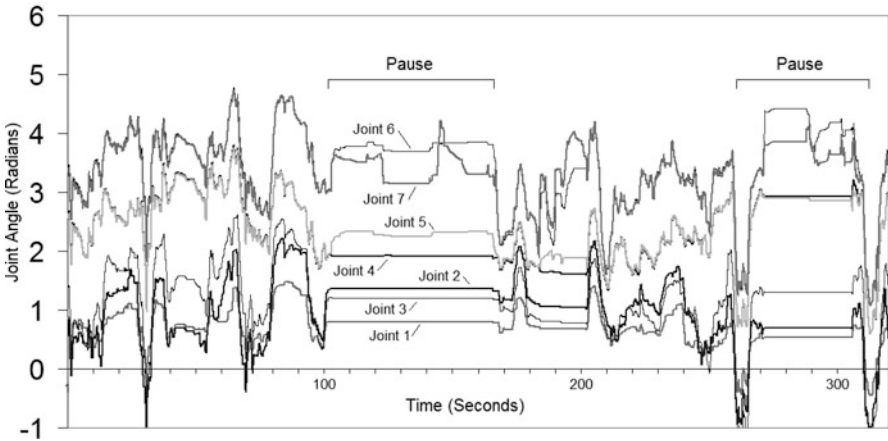


Fig. 15.20 Joint pauses. Bilateral training for subject 5, trial

Fig. 15.21 Joint percentages for velocity and acceleration for all unilateral subjects. Circles and diamonds indicate average values, whiskers indicate the 95% CI

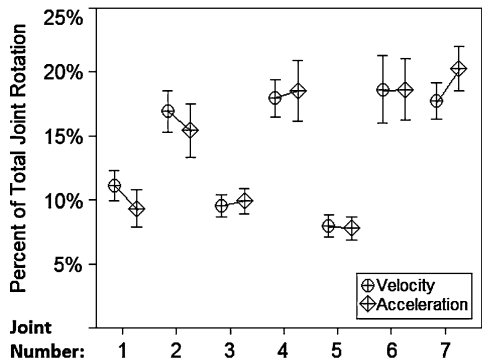


Fig. 15.22 Bilateral percent contributions by joint of the control arm (unimpaired arm), versus the slave (affected) arm given as 95 % CIs with mean values

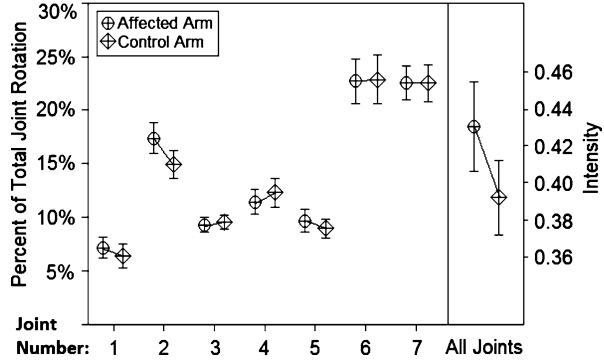
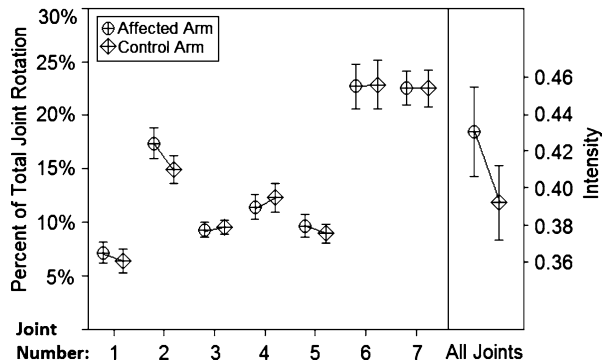


Fig. 15.23 BSRMT versus URMT given as 95 % CIs with mean values



15.4 Discussion

15.4.1 Pilot Study

Patients played the therapy game longer in the bilateral mode with admittance control compared to the unilateral mode and the bilateral group showed more activity for a given therapy session. We can infer that the bilateral with admittance control helped patients spend more time on the therapy compared to the unilateral training group. In physical therapy, it is important to expose the patients to the therapy for as long as possible to maximize the efficiency of the therapy. There is great promise in using assistive methods such as the bilateral with admittance control to improve the therapy results even if it is just by allowing patients to tolerate longer session.

15.4.2 Unilateral vs Bilateral Robotic Training

In this stroke study, there were significant differences in clinical gains following BSRMT versus URMT. The URMT group experienced a greater decrease in tone

and the BSRMT group demonstrated greater gains in ROM. Using the approach described in the Data Analysis section, position, velocity, and acceleration were approximately equivalent measures. This approach also allowed for a more detailed comparative analysis of training. With respect to differences between the less affected control arm and the affected arm for BSRMT, the paretic arm did not always move as far, or as fast as the less affected arm. This difference is explainable by the fact that the robot only provided partial assistance. Recall that the EXO-UL7 only provides a helpful push for the paretic arm. Therefore, for USRMT involving partial assistance, the less affected arm will move more vigorously than the affected arm.

For the Box and Block test, there was a significant improvement for URMT subjects. Given that this test involves grasping blocks and transporting them over a barrier [62], improved performance on the Box and Block test was likely related to grasping improvements: reductions in spasticity in the hand and elbow, as well as improved ROM in the shoulder. The changes in grasping strength for URMT are somewhat puzzling. The EXO-UL7 provides no means to explicitly exercise the hand. Instead, subjects simply grasp a handle while performing training. The EXO-UL7 does not measure gripping force in the hand. Therefore, an explanation for reduced grip strength is somewhat speculative. Notwithstanding, a reduction in hand strength has been associated with reduced spasticity [63]. Thus, like the Box and Block test, reductions in hand strength might relate to reduced spasticity.

The analysis of kinematic data showed that BSRMT was associated with higher velocities of movements in the hand and elbow than URMT. Rapid extension of spastic muscles is generally regarded as undesirable. Thus, if reduction in spasticity of the elbow and/or hand is a therapeutic goal, BSRMT should be avoided. If BSRMT is used, precautions are needed to ameliorate the deleterious effects of rapid symmetric movements on the wrist and elbow. One solution could be to adjust the symmetric control algorithm. This adjustment might limit the joint speeds in the paretic elbow and wrist. However, this would lead to asymmetrical rather than symmetrical movements. An alternative approach could involve a control scheme in which speed is limited for the unaffected arm. For example, providing a viscous sensation in the unaffected wrist and elbow would reduce the velocities in both arms and preserve symmetry. Unilateral robotic training has shown promising results in other stroke studies [11,64,65]. With such precautions in place, BSRMT might have had comparably good results with URMT in terms of reduced spasticity in the elbow and wrist.

Given that all three training groups had some improvement in terms of ROM in the shoulder, these results could be interpreted as an indication that ROM in the shoulder was generally more amenable to an intervention. The range of motion was most improved in the shoulder for the BSRMT. It was significantly improved in the standard care groups but results were mixed for the URMT group. It is not clear how improved shoulder ROM for BSRMT is explainable by a greater cross-talk between the hemispheres of the brain. Indeed, BSRMT is unique from other types of robotic assistance in that the movements are self-guided by the patient. In this respect, the movements imposed on the paretic arm are literally a reflection of how, and when a subject chose to move their arm. Self-generated BSRMT did result in more intense training of the paretic arm. Thus, improvement in ROM may have

resulted simply from greater intensity, and potentially more natural movements of the paretic shoulder. Lacking more direct measures of neurological activities, we find it exceedingly difficult to make conclusions about the effects of robotic training on hemispheric changes in connectivity with kinematic measures alone.

References

1. Kagerer F, Summers J, Semjen A (2003) Instabilities during antiphase bimanual movements: are ipsilateral pathways involved?. *Exp Brain Res* 151:489–500
2. Cattaert D, Semjen A, Summers J (1999) Simulating a neural cross-talk model for between-hand interference during bimanual circle drawing. *Biol Cybern* 81:343–358
3. Yavuzer G, Selles R, Sezer N, Sutbeyaz S, Bussmann J, Koseoglu F, Atay M, Stam H (2008) Mirror therapy improves hand function in subacute stroke: a randomized controlled trial. *Biol Cybern* 89:393–398
4. Sutbeyaz S, Yavuzer G, Sezer N, Koseoglu B (2007) Mirror therapy enhances lower-extremity motor recovery and motor functioning after stroke: a randomized controlled trial. *Arch Phys Med Rehabil* 88(5):555–559
5. Cauraugh J, Kim S, Duley A (2005) Coupled bilateral movements and active neuromuscular stimulation: intralimb transfer evidence during bimanual aiming. *Neurosci Lett* 382(1–2):39–44
6. Simkins M, Fedulow I, Kim H, Abrams G, Byl N, Rosen J (2012) Robotic rehabilitation game design for chronic stroke. *Games Health J* 1(6):422–430
7. Lum P, Burgar C, Shor P, Majmundar M, Loos MVD (2002) Robot-assisted movement training compared with conventional therapy techniques for the rehabilitation of upper-limb motor function after stroke. *Am Congr Rehabil Med Am Acad Phys Med Rehabil* 83:952–959
8. Perry JC, Rosen J, Burns S (2007) Upper-limb powered exoskeleton design. *Mechatronics* 12(4):408–417
9. Perry JC, Rosen J (2006) Design of a 7 degree-of-freedom upper-limb powered exoskeleton. In: *IEEE/RAS-EMBS international conference on biomedical robotics and biomechatronics*, Pisa
10. Krebs HI, Ferraro M, Buerger SP, Newbery MJ, Makiyama A, Sandmann M, Lynch D, Volpe BT, Hogan N (2004) Rehabilitation robotics: pilot trial of a spatial extension for mit-manus. *J NeuroEng Rehabil* 1:5
11. Krebs HI, Hogan N, Aisen ML, Volpe BT (2007) Robot-aided neurorehabilitation: a robot for wrist rehabilitation. *IEEE Trans Neural Syst Rehabil Eng* 15(3):327–335
12. Reinkensmeyer D, Wolbrecht E, Bobrow J (2007) A computational model of human-robot load sharing during robot-assisted arm movement training after stroke. In: *Conf Proc IEEE Eng Med Biol Soc* 2007:4019–4023
13. Majumdar S (1995) *Pneumatic system: principles and maintenance*. Tata McGraw-Hill, New Delhi
14. He J, Koeneman EJ, Schultz RS, Huang H, Wanberg J, Herring DE, Sugar T, Herman R, Koeneman JB (2005) Design of a robotic upper extremity repetitive therapy device. In: *ICORR 2005*, Chicago
15. He J, Koeneman EJ, Schultz RS, Herring DE, Wanberg J, Huang H, Sugar T, Herman R, Koeneman JB (2005) Rupert: a device for robotic upper extremity repetitive therapy. In: *EMBS 2005*, Shanghai
16. Kim H, Miller L, Fedulow I, Simkins M, Abrams G, Byl N, Rosen J (2013) Kinematic data analysis for post-stroke patients following bilateral versus unilateral rehabilitation with an upper limb wearable robotic system. *IEEE Trans Neural Syst Rehabil Eng* 21(2):153–164
17. Perry J, Powell J, Rosen J (2009) Isotropy of an upper limb exoskeleton and the kinematics and dynamics of the human arm. *J Appl Bionics Biomech* 6(2):175–191

18. Rosen J, Perry J (2007) Upper limb powered exoskeleton. *J Humanoid Robot* 4(3):1–20
19. Kim H, Miller L, Rosen J (2011) Redundancy resolution of a human arm for controlling a seven dof wearable robotic system. In: EMBC 2011, Boston
20. Kim H, Li Z, Milutinovic D, Rosen J (2012) Resolving the redundancy of a seven dof wearable robotic system based on kinematic and dynamic constraint. In: ICRA 2012, St. Paul
21. Miller LM, Rosen J (2010) Comparison of multi-sensor admittance control in joint space and task space for a seven degree of freedom upper limb exoskeleton. In: Proceedings of the 3rd IEEE RAS & EMBS international conference on biomedical robotics and biomechatronics, Tokyo, pp 26–29
22. Kallmann M (2008) Analytical inverse kinematics with body posture control. *Comput Animat Virtual Worlds (CAVW)* 19(2):79–91
23. Lee P, Wei S, Zhao J, Badler NI (1990) Strength guided motion. *Comput Graph* 24:253–262
24. Iossifidis I, Steinhage A (2002) Controlling a redundant robot arm by means of a haptic sensor. In: ROBOTIK 2002, pp 269–274
25. Korein JU (1985) A geometric investigation of reach. MIT, Cambridge
26. Perry J, Rosen J (2006) Design of a 7 degree-of-freedom upper-limb powered exoskeleton. In: Proceedings of the 3rd IEEE RAS & EMBS international conference on biomedical robotics and biomechatronics, Pisa, pp 805–810
27. Tsagarakis N, Caldwell DG (2003) Development and control of a ‘Soft-Actuated’ exoskeleton for use in physiotherapy and training. *Auton Robot* 15(1):21–33
28. Wang X (1999) A behavior-based inverse kinematics algorithm to predict arm prehension posture for computer-aided ergonomic evaluation. *J Biomech* 32(5):453–460
29. Zhang X, Chaffin DB (1999) The effects of speed variation on joint kinematics during multisegment reaching movements. *Hum Mov Sci* 18:741–757
30. Yang F, Yuan X (2003) An inverse kinematical algorithm for human arm movement with comfort level taken into account. In: Proceedings of 2003 IEEE conference on control applications, Istanbul, Turkey, pp 1296–1300
31. Garner B, Pandy M (1999) Final posture of the upper limb depends on the initial position of the hand during prehension movements. *Comput Methods Biomech Biomed Eng* 2(2):107–124
32. Badler NI, Tolani D (1996) Real-time inverse kinematics of the human arm. *Presence* 5(4):393–401
33. Craig J (2003) Introduction to robotics: mechanics and control, 3rd edn. Prentice Hall, Harlow, ch 1
34. Yu W, Rosen J, Li X (2011) Admittance control for an upper limb exoskeleton, 2011 american control conference. In: 2011 American control conference – ACC, San Francisco, pp 1124–1129
35. Kim H, Miller LM, Rosen J (2012) Admittance control of seven-dof upper limb exoskeleton to reduce energy exchange. In: ICRA 2012, Saint Paul, pp 1–4
36. Sciavicco L (1987) A dynamic solution to the inverse kinematic problem for redundant manipulators. In: ICRA 1987, vol 4. Raleigh, NC, USA, pp. 1081–1087
37. Sciavicco L (1988) A solution algorithm to the inverse kinematic problem for redundant manipulators. *IEEE Trans Robot Automat* 4(4):403–410
38. Asada H, Granito J (1985) Kinematic and static characterization of wrist joints and their optimal design. In: ICRA 1985, St. Louis, pp 244–250
39. Yoshikawa T (1985) Dynamic manipulability of robot manipulators. In: ICRA 1985, St. Louis, pp 1033–1038
40. Yoshikawa T (1990) Foundations of robotics: analysis and control. MIT, Cambridge
41. Soechting J, Buneo C, Herrmann U, Flanders M (1995) Moving effortlessly in three dimensions: does donders’ law apply to arm movement? *J Neurosci* 15(9):6271–6280
42. Kang T, He J, Tillery SIH (2005) Determining natural arm configuration along a reaching trajectory. *Exp Brain Res* 167:352–361
43. Hogan N (1984) An organizing principle for a class of voluntary movements. *J Neurosci* 4(2):2745–2754

44. Flash T, Hogan N (1985) The coordination of arm movements: an experimentally confirmed mathematical model. *J Neurophysiol* 5:1688–1703
45. Uno Y, Kawato M, Suzuki R (1989) Formation and control of optimal trajectory in human multijoint arm movement – minimum torque-change model. *Biol Cybern* 61:89–101
46. Nakano E, Imamizu H, Osu R, Uno Y, Gomi H, Yoshioka T, Kawato M (1999) Quantitative examinations of internal representations for arm trajectory planning: minimum commanded torque change model. *J Neurophysiol* 81(5):2140–2155
47. Harris CM, Wolpert DM (1998) Signal-dependent noise determines motor planning. *Nature* 391:780–784
48. Todorov E, Jordan MI (2002) Optimal feedback control as a theory of motor coordination. *Nat Neurosci* 5:1226–1235
49. Duma RP, Strick PL (2002) Motor areas in the frontal lobe of the primate. *Physiol Behav* 77:677–682
50. Graziano MS, Taylor CS, Moore T (2002) Complex movements evoked by micro stimulation of precentral cortex. *Neuron* 34:841–851
51. Aerospace medical research laboratory (1975) Investigation of inertial properties of human body, Tech rep, Mar 1975
52. Wada Y, Kaneko Y, Nakano E, Osu R, Kawato M (2001) Quantitative examinations for multi joint arm trajectory planning using a robust calculation algorithm of the minimum commanded torque change trajectory. *J Neural Netw* 14:381–393
53. Biess A, Liebermann D, Flash T (2007) A computational model for redundant human three-dimensional pointing movements: integration of independent spatial and temporal motor plans simplifies movement dynamics. *J Neurosci* 27:13 045–064
54. Li Z, Roldan J, Milutinovic D, Rosen J (2013) The rotational axis approach for resolving the kinematic redundancy of the human arm in reaching movements. In: *EMBC 2013, Osaka*, pp 1–4
55. Secoli R, Milot MH, Rosati G, Reinkensmeyer D (2011) Effect of visual distraction and auditory feedback on patient effort during robot-assisted movement training after stroke. *J Neuroeng Rehabil* 8:21
56. Microsoft. Microsoft robotic developer studio 2008. (Online). Available: <http://www.microsoft.com>
57. Krakauer JW (2006) Motor learning: its relevance to stroke recovery and neurorehabilitation. *Curr Opin Neurol* 19(1):84–90
58. Kato PM (2012) Games for health journal: evaluating efficacy and validating games for health. *Curr Opin Neurol* 1(1):74–76
59. B U S of Public Health. Random error. (Online). Available: sph.bu.edu/otit/MPH-Modules/EP/EP713-RandomError-print.html
60. Taub E, Uswatte G, Pidikiti R (1999) Constraint-induced movement therapy: a new family of techniques with broad application to physical rehabilitation—a clinical review. *J Rehabil Res Dev* 36(3):237–251
61. Andrews A, Bohannon R (1989) Decreased shoulder range of motion on paretic side after stroke. *Phys Ther* 69(9):768–772
62. Mathiowetz V, Volland J, Kashman N, Wever K (1985) Adult norms for the box and block test of manual dexterity. *Am J Occup Ther* 39(6):386–391
63. O’Dwyer N, Ada L, Neilson P (1996) Spasticity and muscle contracture following stroke. *Brain* 119(Pt5):1737–1749
64. Prange G, Jannink M, Groothuis-Oudshoorn C, Hermens H, Ijzerman M (2006) Systematic review of the effect of robot-aided therapy on recovery of the hemiparetic arm after stroke. *J Rehabil Res Dev* 43(2):171–184
65. Norouzi-Gheidari N, Archambault P, Fung J (2012) Effects of robot-assisted therapy on stroke rehabilitation in upper limbs: systematic review and meta-analysis of the literature. *J Rehabil Res Dev* 49:479–496